Physica Scripta

PAPER

Effect of dusty plasma parameters on the low frequency Hall current instability

To cite this article: Sanjib Sarkar *et al* 2023 *Phys. Scr.* **98** 015616

IOP Publishing Phys. Scr. 98 (2023) 015616 https://doi.org/10.1088/1402-4896/acad41

Physica Scripta

CrossMark

RECEIVED
15 October 2022

REVISED
7 December 2022

ACCEPTED FOR PUBLICATION
20 December 2022

PUBLISHED
29 December 2022

PAPER

Effect of dusty plasma parameters on the low frequency Hall current instability

Sanjib Sarkar[1], Jyoti K Atul[2] and Modhuchandra Laishram[3]

[1] Department of Physics, Alipurduar University, West Bengal, India
[2] Upper Atmospheric Sciences Division, Indian Institute of Geomagnetism, Navi Mumbai, India
[3] Department of Physics, College of William and Mary, Williamsburg, Virginia, United States of America

E-mail: sanjibapduphysics@gmail.com

Keywords: dusty plasma, hall current instability, ionosphere, equatorial electrojet

Abstract

The effect of power-law dust size distribution and dust number density on the low frequency hall current instabilities have been studied in and above the equatorial electrojet altitudes using a linear fluid model consisting of electrons, ions and dust particles. The dispersion relation includes electron and ion drift perpendicular to the equilibrium uniform electric and magnetic field, mass and pressure of the charged species and collision between charged and neutral particles. The effect of dust size variation and dust number density on the instability have been investigated by varying the dust-plasma frequency in the dispersion relation. It has been found that in the region of the electrojet altitudes the variation of dust size for the case of broad dust size distribution and dust number density can substantially increase the growth rate and frequency of the instability. However, above the electrojet region where ions become weakly magnetized, the above two dust parameters have a negligible effect on the instability.The present analysis is applicable to the dusty meteor trail plasma of the ionospheric E-region.

1. Introduction

Equatorial electrojet(EEJ) of the ionosphere which is ∼600 km broad in the north-south direction about the magnetic dip equator, can be viewed as a jet of magnetized electrons in the rest frame of the ions and the Earth's fixed frame [1]. EEJ is dynamically controlled by the ionospheric E-region dynamo. Diurnal and semidiurnal tidal oscillation of the atmosphere driven by solar heating is responsible for the E-region dynamo which leads to strong current flows in the east-west direction around the magnetic dip equator in the altitude range of ∼90 km to ∼120 km [1]. The electric field associated with the EEJ is not only self generated by the local wind field but also by the global dynamo effect [1]. EEJ is unstable mainly due to Type-I and Type-II irregularities [2, 3].The radar back scattered frequency spectra from the field aligned irregularities are classified into type-I and type-II irregularities. In a collisionless unmagnetized plasma with equal electron and ion temperatures, the two-stream instability occurs when the mean velocity of the electrons relative to the ions exceeds the thermal velocity of the electrons and the resulting perturbing waves travel at a velocity that is approximately equal to ion acoustic velocity. Wave grows when the particles travel slightly faster than the wave phase velocity and on the other hand, wave is damped when the particles travel at almost the same velocity as the wave. However, the physical mechanism involved in classic two stream instability fails to explain the irregularities which were observed in the ionosphere due to the effect of collisions between charged and neutral particles and the presence of the geomagnetic field. Type-I irregularities were first explained theoretically by Farley [4] and Buneman [5] by extending the theory of two-stream plasma ion wave instability via including the effect of neutral collision and static magnetic field in weakly ionized plasma in which electrons are magnetized and ions are unmagnetized. Type-II irregularities are driven by the density and electrical potential gradients [6].

In the EEJ of the ionosphere at the altitude range of ∼95 km to ∼ 115 km, Farley-Buneman (FB) instability or high frequency hall current instability was first observed by 50 MHz radar backscattering at Jicamarca, Peru

[7] and subsequently observed and investigated by many other several researchers [8–20]. In the EEJ region, electrons are strongly magnetized whereas ions are unmagnetized because at these altitudes electron gyrofrequency is much larger than the electron-neutral collision frequency and ion gyrofrequency is much smaller than the ion-neutral collision frequency [18]. If the equilibrium electric field, $\mathbf{E}_0$ exists perpendicular to $\mathbf{B}$, it leads to a cross-field $\mathbf{E}_0 \times \mathbf{B}$ two-stream instability. The instability is excited when the electron drift speed exceeds the ion acoustic speed and it propagates in the direction of the cross-field drift of electrons. The perpendicular drift is found to be much larger than the drifts parallel to $\mathbf{B}$. Since the ions are unmagnetized in the EEJ region, the ion's drift is almost entirely in the direction of $\mathbf{E}_0$ and is much smaller than the ion thermal velocity. Therefore, ion's drift can be neglected in the EEJ region.

In the higher latitudes (above∼120 km), FB instability is also observed around the polar cap or auroral Zone [1]. Moreover, it has been shown that at such higher altitudes the ion thermal effect reduces the threshold for the electrojet instabilities but increases the maximum altitude of the instabilities [20]. The instabilities in the central electrojet (which is below the boundary of ion magnetization) are predominantly determined by the FB driving mechanism. Above the ion magnetization boundary, ions build up considerable hall current and the relative drift between ions and electrons plays a significant role in the instability. At these altitudes, since ion magnetization is important, ion cross-field drifts cannot be neglected [20].

For the past three decades, dusty plasma has been an active research field due to its immense importance in Laboratory, Industry and Space [21–23]. Apart from the usual plasma electrons, ions and neutral gas, dusty plasma consists of additional charged dust species of radii between nm to a few micrometers. Dusty plasma naturally occurs in different space and astrophysical environments, examples include such as interstellar medium [24], protoplanetary disks [25], rings of Saturn [26], cometary environments [27] and D and E-region of the Ionosphere [28–48]. Since charged dust in the ionospheric regions can influence the incoherent scattering of radio waves from different ionospheric layers which are used for radio communication and signal processing, it is important to understand the physics of ionospheric dusty plasma [28, 29].

The upper D (of altitude ∼75 to ∼90 km) or lower E region (of altitude ∼90 to ∼130 km) of the ionosphere can be considered as a partially ionized low temperature natural dusty plasma laboratory in which minimum temperature in the summer mesopause can be as low as in the range of 100 k to 150 k [28]. Due to the ablation of meteors at the altitude range of ∼75 km to ∼115 km, fine dust particles form and produce dust layers. Noctilucent clouds (NLC) and Polar Mesospheric Clouds (PMC) or Polar Mesospheric Summer Echoes (PMSE) are fascinating examples of dust layers [28, 29]. PMSE is related to the strong radar echoes due to the electron scattering at 50–1.3 GHz, which is observed at altitudes of ∼78 km − ∼ 80 km above the NLC region, formed due to water-ice particles [28, 29, 33–35, 39–41, 43–45]. The density and radius of the ice particles can vary between $10 - 10^3$ cm^{-3} and 1-100 nm respectively [28].

At altitudes about ∼80 km–∼120 km, sputtered particles in the vicinity of meteoroid form ionized meteor trails which can be observed optically as well as by the radar backscattering [28]. While probing the ionosphere with radars, meteor produce mainly three types of returns. The first radar detection occurs when meteor trails are in the direction perpendicular to the radar beams. The second type is associated with the short duration pulse periods known as head echoes and the third type is meteor echoes returns from the meteor trail which is not perpendicular to the radar beam [49].Chapin and Kudeki [50] observed the nonspecular meteor trails and interpreted their origin by electrojet instabilities, in particular, FB instability.

Kelly *et al* [51] identified the meteor trail and shows that ablated material in the trail may coagulate into a particle of an order of 50 nm radius. It is believed that ablation and recondensation leads to the formation of many smaller dust particles. However, there are large uncertainties regarding the dust size, number density and compositions. For example, Reitmeijer *et al* [52] found dust sizes >100nm, but Mateshvili *et al* [53], found dust sizes of 10nm and number densities of 30 cm^{-3} at ∼117 km height followed by Leonid meteor showers. Moreover, the work of Rosinski and Snow [54] and Hunten *et al* [55] show the height and size distribution of dust particles which are formed during the meteor ablation process and its subsequent evolution through coagulation, sedimentation and diffusion. They estimated that the dust particle radii were in a submicron size range with densities of a few 1000 cm^{-3} and these dust particles could exist upto an altitude of 110 km.

Neutral dust particles can modify the E-region (of altitude range from ∼90 km to ∼120 km) conductivities due to collision frequencies with charged particles in addition with ion-neutral and electron-neutral collision frequencies [36]. If the height distribution of the dust number density is known, it can explain the theoretical estimates of the height difference between the current and the conductivity peaks [36]. Instead of neutral dust particles if these are negatively charged, it can decrease the number density of free electrons below the EEJ peak in which the number density of meteoric dust particles are very high. Due to the reduction of the free electron number density, it can decrease or reverse the normal electrojet currents (known as counter electrojet) below the peak of the EEJ [37, 38].

Since dust particles are charged, dusty plasma supports various kinds of waves and instabilities. When these charged dust particles constitute uniform fixed background, normal ion acoustic mode gets modified and gives dust-ion acoustic mode [56]. Another extremely low frequency wave exists (due to the massive dust grains compared to the negative ions), which involves dust dynamics, called dust acoustic wave [57], and was first clearly observed in the laboratory by Barkan *et al* [58]. Dust acoustic instability spontaneously excited when ion drift velocity relative to dust exceeds wave phase velocity. Since dust particles are massive compared to ions, dust acoustic speed is typically a few cm s^{-1} and frequency is a few Hz.

Dusty waves and instabilities in the context of EEJ were first discussed by Rosenberg and Chow [59]. It has been shown that charged dust can modify the usual Farley-Buneman and Gradient drift mode through its effect via equilibrium charge neutrality in the EEJ region [59, 60]. Considering dust dynamics and using kinetic theory Rosenberg and Shukla [61], investigated low frequency hall current instability. The instability is very likely to be excited for sufficient density of positively charged dust in which electron $\mathbf{E}_0 \times \mathbf{B}$ drift speed is smaller than the ion thermal speed. Dust particles are usually negatively charged in the laboratory (due to fast moving electrons compared to ions) but in space environments, it may become positive due to photo emission in the presence of solar UV radiation if the dust particles work function is sufficiently low [21, 46]. Rosenberg and shukla [61] developed the theory for the EEJ altitudes ($\sim$95 $km - \sim$ 105 km), in which only electrons are magnetized while ions and dust particles are unmagnetized. However, it has been shown that dust particles may exist upto an altitude of $\sim$130km, due to the transportation of dust particles by dust vortices (formed at altitudes $\sim$110 km $- \sim$ 120 km) which appear as a result of acoustic gravity wave instability [62].

Now, above the EEJ altitude since ions are also weakly magnetized due to lower neutral density, it may influence the low frequency hall current instability. N. D' Angelo discussed the FB instability and low frequency dust acoustic hall current instability in the case for which both electrons and ions are magnetized but only dust particles are unmagnetized at the altitude of $\sim$100 km to $\sim$120 km for uniform 50 nm size dust [63]. However, it is evident from the several observations as discussed above that the dust sizes may vary and modify the wave propagation at these altitudes. Therefore, it is important to see the effect of dust size variation on the low frequency hall current instability.

Early investigation of dust size distribution in dusty plasma was given by Havness *et al* [64]. It has been shown that the effect of dust size distribution can strongly influence the dust charges and potential in the dust cloud. Effect of dust size distribution on low frequency dust acoustic wave was addressed by Brattli *et al* [65]. They found that despite of different power law exponent, if the upper and lower limits of dust particle sizes are chosen such that average dust sizes remain constant, wave properties are similar to those of monosize distribution of the average size dust particles. Meuris showed that dust plasma frequency increases for power law or normal dust size distribution as compared to the case of monosized dust particles [66]. Further, it has been shown that soliton velocity in dusty plasma increases with power law dust size distribution compared to the case for monosized dust particles [67]. Also, the effect of the power-law dust size distribution on linear dust acoustic wave in inhomogeneous unmagnetized dusty plasma has been carried out by Banerjee *et al* [68]. It has been shown that dust size distribution and density inhomogeneity can significantly affect wave properties.

Since the charged dust naturally occurs in the meteor ablation region (80–120 km), it can affect the well known E-region instabilities such as the Farley-Buneman instability or Hall current instability. The effect of charged dust on Hall current instability can be studied by two approaches:

(i) One approach is by considering the cold dust fluid which constitutes stationary background and it affects the instability via altering the plasma quasineutrality condition. This effect manifests itself through the modification of the ion waves [59].

(ii) The other method is to consider dust dynamics which results a low frequency Hall current instability in which the frequency is within the range of dust acoustic wave.

Since we are interested in the low frequency analog of the Hall current instability later approach is considered in this work. Now, since naturally dust sizes may vary due to the complex meteoric ablation process, the present work aimed to address how the variable size charged dust particles can affect the low frequency Hall current instability in and above the electrojet region.

In this paper, the effect of power law dust size distribution and dust number density on the low frequency hall current instability in and above the electrojet region has been carried out. Specifically, the growth rate and frequency of the instability at different altitude ranges(in which only electrons are magnetized in one case and other two cases for strongly magnetized electrons and weakly magnetized ions) have been evaluated numerically. The article is organized as follows: section 2 describes a basic mathematical model which includes equilibrium coordinate geometry, model assumptions, fluid dispersion relation and dust-plasma frequency for power law dust size distribution. The effect of dusty plasma parameters on the instability is presented in section 3 which consists of the effect of power law dust size distribution in and above the EEJ altitude and the effect of dust number density. In section 4, analytical expressions for the growth rate and frequency of the instability in the EEJ region have been derived. Discussion and conclusion are given in section 5 and section 6 respectively.

2. Basic mathematical model

Let us consider a partially ionized dusty plasma consisting of electrons, singly charged ions, variable-size dust particles and neutral gas molecules. The density, temperature, mass and velocity of each species are denoted by n_α, T_α, m_α and V_α where $\alpha = d, e, i, n$ stands for the dust particles, electrons, ions and neutrals respectively.

In space plasma, mostly dust size distribution is modeled by a power-law distribution for dust radii r vary within a given range (r_{min}, r_{max}). The distribution has the following form [64–68]:

$$n(r)dr = Kr^{-\beta}dr, \tag{1}$$

where K is a constant and the values of the exponent β vary from 0.9 to 4.5 for planetary system [69], for the cometary environment, the value of β is ~3.4 [66]. For $r < r_{min}$ and $r > r_{max}$, $n(r) = 0$, the total number density of the dust particle is given by,

$$N_{tot} = \int_{r_{min}}^{r_{max}} n(r)dr. \tag{2}$$

The value of K in the equation (1) can be determined as follows:

$$K = \frac{(1-\beta)N_{tot}}{r_{max}^{1-\beta} - r_{min}^{1-\beta}}. \tag{3}$$

The charge neutrality at equilibrium is given by

$$n_{io} = \varepsilon\sum_{j=1}^{N} n_{doj}Z_{dj} + n_{eo}, \tag{4}$$

where, $j = 1, 2, 3, \ldots, N$ are N different species of dust grains. n_{i0}, n_{e0} and n_{d0j} are the equilibrium unperturbed ion, electron and the dust particle number density respectively. Z_{dj} represents the number of charges residing on the jth dust particle. The expression for Z_{dj} and m_{dj} are as follows:

$$Z_{dj} \approx 4\pi\varepsilon_0 v_0 r_j/e, \tag{5}$$

$$m_{dj} \approx \frac{4}{3}\pi\rho_d r_j^3, \tag{6}$$

where ϵ_0 is the free space permittivity, ρ_d is the mass density of the dust particle and v_0 is the equilibrium dust surface potential. v_0 and ρ_d are assumed to be the constant for all dust particle sizes.

In equation (4), $\epsilon = 1$ for negatively charged dust and -1 for the positively charged dust. The parameter, $\delta = \frac{n_i}{n_e}$ represents the amount of charge density carried by the dust particle. All the dust particle sizes r are assumed to be much smaller than the dust debye length, $r \ll \lambda_{Dd}$.

2.1. Equilibrium coordinate geometry of the model

The coordinate system for the electric and magnetic fields for the study of low frequency hall current instability in the presence of variable size dust particle is same as in [61]. The magnetic field, **B** is in the *z* direction whereas the electric field, $\mathbf{E}_0$ is in the $-$x direction. The electrons and ions have $\mathbf{E}_0 \times \mathbf{B}$ drift in the perpendicular direction. The electron and ion drift parallel to the direction of $\mathbf{E}_0$ is neglected. Since ion and dust particles are unmagnetized in the EEJ region, the ion and dust drifts are neglected whereas in above the electrojet region (~115 km $-$ ~ 130 km), ion drift is considered together with electron drift due to the weakly magnetized ions (see figure 1) because in these region, $\nu_{in} \gtrsim \Omega_i$ or $\nu_{in} \lesssim \Omega_i$. However, if the ions are strongly magnetized (such as in F region), $\nu_{in} \ll \Omega_i$, although electrons and ions gyrate in the opposite direction, but their guiding center drifts are charge independent and move in the same direction which inhibits the formation of current [20, 70].

2.2. Model assumptions

In the EEJ region following assumptions have been made to develop the model:

(1) The electrons are magnetized and ions and dust particles are unmagnetized.

(2) Only electrostatic waves are considered.

(3) Due to higher concentration of neutral gases, coulomb collisions between charged species are smaller than the collision between neutral gases and plasma particles. Hence, collision between charged species is neglected.

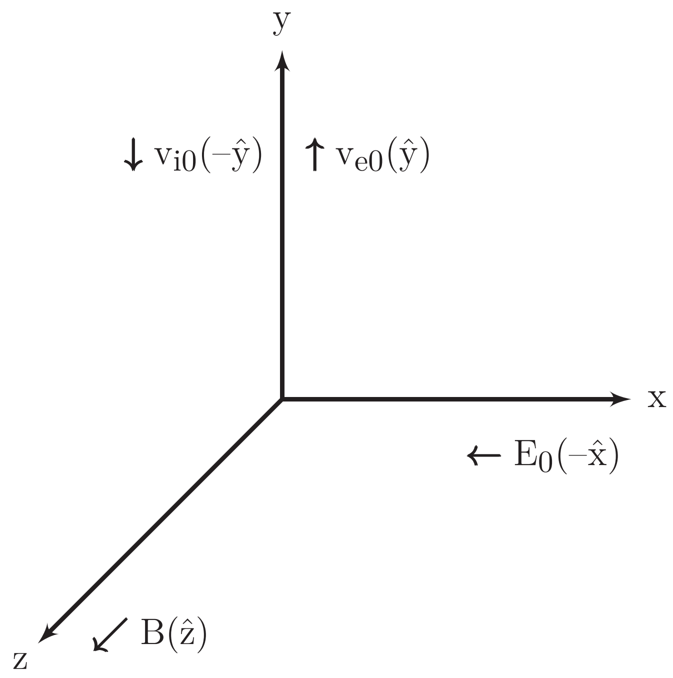

Figure 1. Equilibrium field geometry of the model

(4) No neutral wind is considered.

(5) The frequency regime, $\omega \gg \Omega_d$ is considered.

(6) The equilibrium plasma density and temperature gradients are not considered.

However above the EEJ, due to lower neutral density, ν_{in} can be comparable or lower than Ω_i. Therefore ion's drift can not be neglected in this region. Low frequency hall instability in the above EEJ region is also considered in this work.

2.3. Fluid dispersion relation

Since, we are interested in the time scale that is long in comparison with the microscopic particle dynamics and for a wavelength that is also much larger than the characteristic plasma debye length, fluid description of the charged particle species in a plasma is sufficient. The fluid description of plasma considers the average value of the macroscopic variables such as density, velocity, temperature etc which are related to the moments of the distribution function. Waves and instabilities in dusty plasma can be analyzed by considering dust as another fluid component in addition to the electron and ion fluid. However, for the shorter wavelength of the instability, one requires kinetic theory.

To obtain the fluid dispersion relation for electrostatic low frequency hall instability in and above the EEJ region, the continuity and momentum equations for the three charged components are as follows:

$$\frac{\partial}{\partial t} n_\alpha + \nabla(n_\alpha \mathbf{V}_\alpha) = 0, \quad (7)$$

$$n_\alpha m_\alpha \frac{d\mathbf{V}_\alpha}{dt} = n_\alpha q_\alpha (\mathbf{E} + \mathbf{V}_\alpha \times \mathbf{B}) - kT_\alpha \nabla n_\alpha - n_\alpha m_\alpha \nu_{\alpha n} \mathbf{V}_\alpha, \quad (8)$$

where, $\alpha = e, i, d$ stands for the electron, ion and dust particles respectively. Here in equation (8), we have not considered the gravity, which is much smaller compared to the other terms. $\frac{d}{dt}$ is the convective derivative. The right hand side of the momentum equation (8) contains Lorentz force term which leads to the Hall term, pressure gradient term and the third term stands for the collisional momentum exchange of charged species with the neutrals. Without considering dust, assuming inertia less electrons and plasma quasineutrality ($n_e = n_i$), one can obtain the expression for the electric field from the momentum equation (8) in the rest frame of ions which contains the hall term ($\mathbf{J} \times \mathbf{B}/en_e$, where $\mathbf{J}(= en_e(\mathbf{v_i} - \mathbf{v_e}))$ is the current density) [71]. In a partially ionized medium such as in the E region of the ionosphere, the Hall effect occurs owing to the fact that neutral collisions more efficiently isolate ions from the magnetic field than the electrons which is different from the case of highly ionized plasma in which the Hall effect arises simply due to the difference between electron and ion inertia [71]. Furthermore, in the case of dusty plasma, since charged dust affects the plasma quasineutrality ($n_e \neq n_i$), the Hall effect will always exist even in the absence of relative drift between electrons and ions unless the condition $Zn_d \ll n_e$ is satisfied [72].

Since, we are interested to study the Hall current instability, the parameters such as plasma density, velocity, magnetic field etc that govern the instability can be easily understood during its initial phase. Mathematically, this can be done by linearizing the continuity and momentum equations by introducing infinitesimal perturbations. The solution of the linearized system of equations gives the dispersion relation which can be presented in a simple functional form, $f(\omega, k) = 0$.

Equations (7) and (8) can be linearized as follows: $n_\alpha = n_{\alpha 0} + \lambda n_{\alpha 1}$, $\mathbf{V_\alpha} = \mathbf{V_{\alpha 0}} + \lambda \mathbf{V_{\alpha 1}}$, $T_\alpha = T_{\alpha 0} + \lambda T_{\alpha 1}$, and $\mathbf{E} = \mathbf{E}_0 - \lambda \nabla\phi$,

where λ and ϕ are the infinitesimal expansion parameter and the perturbing potential respectively. All other symbols have their usual meaning in which the first part represents equilibrium part and the second one is perturbing quantities that are assumed to be small as compared to the equilibrium value.

From the zeroth order linearized equation corresponding to the equations (7) and (8), we obtain the expression for the equilibrium drift velocities which are as follows:

$$V_{\alpha ox} = -\frac{q_\alpha}{m_\alpha}\frac{\nu_{\alpha n}}{\Omega_\alpha^2 + \nu_{\alpha n}^2}E_0, \tag{9}$$

$$V_{\alpha 0y} = -\frac{q_\alpha}{m_\alpha}\frac{\Omega_\alpha}{\Omega_\alpha^2 + \nu_{\alpha n}^2}E_0, \tag{10}$$

and

$$V_{\alpha 0z} = 0. \tag{11}$$

Where, c_α and Ω_α are the species thermal velocity and gyrofrequency respectively. Combining the zeroth and first order terms in the momentum equation (8), we get,

$$n_{\alpha 0}m_\alpha\left(\frac{\partial}{\partial t}\mathbf{V}_{\alpha 1} + \mathbf{V}_{\alpha 0}.\nabla\mathbf{V}_{\alpha 1}\right) = n_{\alpha 0}q_\alpha(-\nabla\phi + \mathbf{V}_{\alpha 1}\times\mathbf{B}) - \nabla P_{\alpha 1} - n_{\alpha 0}m_\alpha\nu_{n\alpha}\mathbf{V}_{\alpha 1}. \tag{12}$$

Let's assume that first order quantities vary as $\sim\exp\{i(k_x x + k_y y - \omega t)\}$. It is also assumed that the perturbing low frequency waves propagate predominantly along the y- axis ($k_x \ll k_y$). From equation (12) by considering the k_y terms we get,

$$n_{\alpha 0}(-i\omega\mathbf{V}_{\alpha 1} + V_{\alpha 0y}ik_y\mathbf{V}_{\alpha 1}) = -\frac{n_{\alpha 0}q_\alpha ik_y\phi}{m_\alpha} + \frac{n_{\alpha 0}q_\alpha}{m_\alpha}\mathbf{V}_{\alpha 1}\times\mathbf{B} - \frac{\nabla P_{\alpha 1}}{m_\alpha} - n_{\alpha 0}\nu_{\alpha n}\mathbf{V}_{\alpha 1}. \tag{13}$$

Separating into the x and y components, we get

$$(\omega - k_y V_{\alpha 0y} + i\nu_{\alpha n})V_{\alpha 1x} = \frac{q_\alpha}{m_\alpha}k_x\phi + i\Omega_\alpha V_{\alpha 1y} + c_\alpha^2 k_x\frac{n_{\alpha 1}}{n_{\alpha 0}}, \tag{14}$$

$$(\omega - k_y V_{\alpha 0y} + i\nu_{\alpha n})V_{\alpha 1y} = \frac{q_\alpha}{m_\alpha}k_y\phi - i\Omega_\alpha V_{\alpha 1x} + c_\alpha^2 k_y\frac{n_{\alpha 1}}{n_{\alpha 0}}, \tag{15}$$

From the above two equations, one obtains

$$\hat{\omega}_\alpha V_{\alpha 1x} - i\Omega_\alpha V_{\alpha 1y} = \frac{q_\alpha}{m_\alpha}k_x\phi + c_\alpha^2 k_x\frac{n_{\alpha 1}}{n_{\alpha 0}}, \tag{16}$$

and

$$\hat{\omega}_\alpha V_{\alpha 1y} + i\Omega_\alpha V_{\alpha 1x} = \frac{q_\alpha}{m_\alpha}k_y\phi + c_\alpha^2 k_y\frac{n_{\alpha 1}}{n_{\alpha 0}}, \tag{17}$$

where, $\hat{\omega}_\alpha = (\omega - k_y V_{\alpha 0y} + i\nu_{\alpha n})$.

Now from the above two equations, one can get the expression for $V_{\alpha 1x}$ and $V_{\alpha 1y}$.

$$(\hat{\omega}_\alpha^2 - \Omega_\alpha^2)V_{\alpha 1x} = \frac{q_\alpha\phi}{m_\alpha}(ik_y\Omega_\alpha + \hat{\omega}_\alpha k_x) + c_\alpha^2\frac{n_{\alpha 1}}{n_{\alpha 0}}(ik_y\Omega_\alpha + \hat{\omega}_\alpha k_x), \tag{18}$$

$$(\Omega_\alpha^2 - \hat{\omega}_\alpha^2)V_{\alpha 1y} = \frac{q_\alpha\phi}{m_\alpha}(ik_x\Omega_\alpha - \hat{\omega}_\alpha k_y) + c_\alpha^2\frac{n_{\alpha 1}}{n_{\alpha 0}}(ik_x\Omega_\alpha - \hat{\omega}_\alpha k_y). \tag{19}$$

After linearizing the continuity equation (7) to the first order, we get

$$n_{\alpha 1} = \frac{n_{\alpha 0}}{(\omega - k_y V_{\alpha 0y})}(k_x V_{\alpha 1x} + k_y V_{\alpha 1y}). \tag{20}$$

Substituting the values of $V_{\alpha 1x}$ and $V_{\alpha 1y}$ from equations (18)and (19), we obtain,

$$n_{\alpha 1} = \frac{\hat{\omega}_\alpha k^2 \phi n_{\alpha 0} q_\alpha}{m_\alpha(\hat{\omega}_\alpha^2 - \Omega_\alpha^2)(\omega - k_y V_{\alpha 0y}) - m_\alpha \hat{\omega}_\alpha k^2 c_\alpha^2}, \tag{21}$$

where, $k^2 = k_x^2 + k_y^2$ and $k_x \ll k_y$.

Now for electrons, ions and negatively charged dust the corresponding expression for $n_{\alpha 1}$ becomes,

$$n_{e1} = -\frac{\hat{\omega}_e k^2 \phi n_{e0} e}{m_e(\hat{\omega}_e{}^2 - \Omega_e^2)(\omega - k_y V_{e0y}) - m_e \hat{\omega}_e k^2 c_e^2}, \tag{22}$$

$$n_{i1} = \frac{\hat{\omega}_i k^2 \phi n_{i0} e}{m_i(\hat{\omega}_i{}^2 - \Omega_i^2)(\omega - k_y V_{i0y}) - m_i \hat{\omega}_i k^2 c_i^2}, \tag{23}$$

$$n_{d1} = -\frac{\hat{\omega}_d k^2 \phi n_{d0} Z_d e}{m_d(\hat{\omega}_d{}^2 - \Omega_d^2)(\omega - k_y V_{d0y}) - m_d \hat{\omega}_d k^2 c_d^2}. \tag{24}$$

The dispersion relation is obtained through the linearized Poisson's equation,

$$\varepsilon_0 \nabla^2 \phi = -e(n_{i1} - n_{e1} - Z_d n_{d1}). \tag{25}$$

Since the perturbing potential ϕ varies as $\sim \exp\{i(k_x x + k_y y - \omega t)\}$, $(k_x \ll k_y)$, the above equation yields,

$$1 + \sum_{\alpha = e,i,d} \chi_\alpha = 0, \tag{26}$$

where $\chi_e = \frac{e n_{e1}}{\varepsilon_0 k^2 \phi}$, $\chi_i = -\frac{e n_{i1}}{\varepsilon_0 k^2 \phi}$, $\chi_d = \frac{e Z_d n_{d1}}{\varepsilon_0 k^2 \phi}$ represents electron, ion and dust susceptibilities respectively. Now, from equations (22)–(26), one can obtain the expression for χ_e, χ_i and χ_d.

$$\chi_e = -\frac{\omega_{pe}^2 \hat{\omega}_e}{(\hat{\omega}_e{}^2 - \Omega_e^2)(\omega - k_y V_{e0y}) - \hat{\omega}_e k^2 c_e^2}, \tag{27}$$

similarly for the ions, we get

$$\chi_i = -\frac{\omega_{pi}^2 \hat{\omega}_i}{(\hat{\omega}_i{}^2 - \Omega_i^2)(\omega - k_y V_{i0y}) - \hat{\omega}_i k^2 c_i^2}, \tag{28}$$

and for the negatively charged dust,

$$\chi_d = -\frac{\omega_{pd}^2 \hat{\omega}_d}{(\hat{\omega}_d{}^2 - \Omega_d^2)(\omega - k_y V_{d0y}) - \hat{\omega}_d k^2 c_d^2}. \tag{29}$$

Case-1: From equations (26)–(29), the resulting dispersion relation for the negatively charged dust becomes

$$1 + \chi_e + \chi_i + \chi_d = 0, \tag{30}$$

$$1 - \frac{\omega_{pe}^2 \hat{\omega}_e}{(\hat{\omega}_e{}^2 - \Omega_e^2)(\omega - k_y V_{e0y}) - \hat{\omega}_e k^2 c_e^2} - \frac{\omega_{pi}^2 \hat{\omega}_i}{(\hat{\omega}_i{}^2 - \Omega_i^2)(\omega - k_y V_{i0y}) - \hat{\omega}_i k^2 c_i^2} - \frac{\omega_{pd}^2 \hat{\omega}_d}{(\hat{\omega}_d{}^2 - \Omega_d^2)(\omega - k_y V_{d0y}) - \hat{\omega}_d k^2 c_d^2} = 0. \tag{31}$$

Case-2: Now for the positively charged dust, the linearized Poisson's equation has the following form,

$$\varepsilon_0 \nabla^2 \phi = -e(n_{i1} - n_{e1} + Z_d n_{d1}), \tag{32}$$

Equation (32) can be rearranged in the form of equation (26), where, $\chi_e = \frac{e n_{e1}}{\varepsilon_0 k^2 \phi}$, $\chi_i = -\frac{e n_{i1}}{\varepsilon_0 k^2 \phi}$, and $\chi_d = -\frac{e Z_d n_{d1}}{\varepsilon_0 k^2 \phi}$. Now for positively charged dust since $q_d = Z_d e$, n_{d1} should contain positive sign (see equation (21)).The sign of the expressions for n_{e1} and n_{i1} remain the same as equations (22) and (23). Therefore, we get the same dispersion relation both for the positively and the negatively charged dust. From equation (31), we can write

$$\begin{aligned}
&\{(\hat{\omega}_e^2 - \Omega_e^2)(\omega - k_y V_{e0y}) - \hat{\omega}_e k^2 c_e^2\} \\
&\{(\hat{\omega}_i{}^2 - \Omega_i^2)(\omega - k_y V_{i0y}) - \hat{\omega}_i k^2 c_i^2\}\{(\hat{\omega}_d^2 - \Omega_d^2)(\omega - k_y V_{d0y}) - \hat{\omega}_d k^2 c_d^2\} \\
&-\omega_{pe}^2 \hat{\omega}_e \{(\hat{\omega}_i{}^2 - \Omega_i^2)(\omega - k_y V_{i0y}) - \hat{\omega}_i k^2 c_i^2\}\{(\hat{\omega}_d^2 - \Omega_d^2)(\omega - k_y V_{d0y}) - \hat{\omega}_d k^2 c_d^2\} \\
&-\omega_{pi}^2 \hat{\omega}_i \{(\hat{\omega}_e^2 - \Omega_e^2)(\omega - k_y V_{e0y}) - \hat{\omega}_e k^2 c_e^2\}\{(\hat{\omega}_d^2 - \Omega_d^2)(\omega - k_y V_{d0y}) - \hat{\omega}_d k^2 c_d^2\} \\
&-\omega_{pd}^2 \hat{\omega}_d \{(\hat{\omega}_e^2 - \Omega_e^2)(\omega - k_y V_{e0y}) - \hat{\omega}_e k^2 c_e^2\}\{(\hat{\omega}_i^2 - \Omega_i^2)(\omega - k_y V_{i0y}) - \hat{\omega}_i k^2 c_i^2\} = 0.
\end{aligned} \tag{33}$$

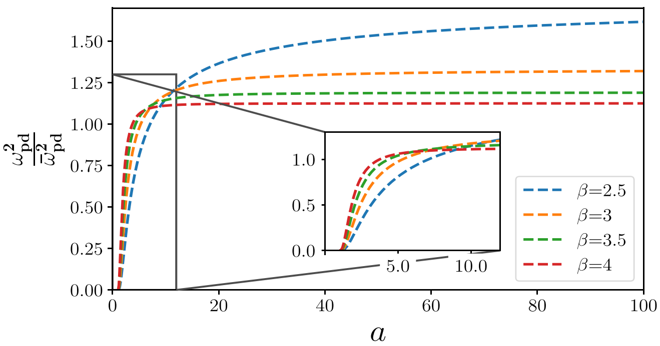

Figure 2. The variation of $\frac{\omega_{pd}^2}{\bar{\omega}_{pd}^2}$ with respect to $a(=\frac{r_{max}}{r_{min}})$ for different β.

Since ω is complex, let's assume

$$\omega = \omega_r + i\gamma_r, \tag{34}$$

where ω_r is the real frequency and γ_r is the corresponding growth rate. After substituting equation (34) in equation (33), one can obtain the real and imaginary parts of the dispersion relation. The dispersion relation is solved numerically using PYTHON3 for the case of variation of dust size and dust number density, n_d in and above the EEJ region.

2.4. Dust-plasma frequency(ω_{pd}) for power law dust size distribution

The effect of dust size variation is included through ω_{pd}^2 in equation (33). For the dust size variation, one can write,

$$\omega_{pd}^2 = \frac{e^2}{\varepsilon_0}\sum_{j=1}^{N}\frac{n_{doj}(r)Z_{dj}^2}{m_{dj}}, \tag{35}$$

where n_{doj}, Z_{dj} and m_{dj} are unperturbed dust density, dust charge state and dust mass of the jth dust grain respectively. For the power law distribution of continuous cases, we get from equation (1),

$$\omega_{pd}^2 = \frac{12\pi\varepsilon_0 v_0^2}{\rho_d\beta}K(r_{min}^{-\beta} - r_{max}^{-\beta}). \tag{36}$$

The average values of r can be written as

$$\bar{r} = K\int_{r_{min}}^{r_{max}} r^{-\beta+1}dr/N_{tot}. \tag{37}$$

From equation (3), we get

$$\bar{r} = \frac{1-\beta}{2-\beta}\left(\frac{r_{max}^{2-\beta} - r_{min}^{2-\beta}}{r_{max}^{1-\beta} - r_{min}^{1-\beta}}\right), \tag{38}$$

so that,

$$\bar{\omega}_{pd}^2 = \frac{12\pi\varepsilon_0 v_0^2}{\rho_d\beta}\frac{N_{tot}}{\bar{r}}, \tag{39}$$

where, $\bar{\omega}_{pd}$ is the average dust plasma frequency. From equations (36) and (39), we have

$$\frac{\omega_{pd}^2}{\bar{\omega}_{pd}^2} = \frac{(\beta-1)^2(a^{-\beta}-1)(a^{2-\beta}-1)}{\beta(\beta-2)(a^{1-\beta}-1)^2}, \tag{40}$$

where, $a = \frac{r_{max}}{r_{min}}$. Equation (40) shows that the ratio of the dust-plasma frequency, ω_{pd} for power law dust size distribution with average dust plasma frequency, $\bar{\omega}_{pd}$ for average size dust depends on the ratio of the maximum dust size, r_{max} to the minimum dust size, r_{min} and the power law exponent β. Since ω_{pd} differs from the, $\bar{\omega}_{pd}$, it characterizes the power law dust size distribution.

The variation of $\frac{\omega_{pd}^2}{\bar{\omega}_{pd}^2}$ is plotted with respect to a for different values of β in figure 2. From figure 2, it can be seen that as a increases $\frac{\omega_{pd}^2}{\bar{\omega}_{pd}^2}$ is increased but it decreases as the β increases. However, upto $a \approx 8$, the ratio $\frac{\omega_{pd}^2}{\bar{\omega}_{pd}^2}$ sharply increases with a and also with the increase of β (see inset plot in figure 2). Since the altitude range from ~95 km to ~130 km considered in this paper, the dust size may vary from a few nm to several tens of nm, it is

Table 1. Ionospheric plasma parameters.

Symbol	Reference/Formula	Magnitude at EEJ Altitude Range (∼95 km–∼105 km)	Magnitude above EEJ	
			Altitude Range (∼115 km–∼120 km)	Altitude Range (∼125 km–∼130 km)
N_n	[1, 76]	$10^{13}(cm^{-3})$	$7.8\times10^{11}(cm^{-3})$	$2.8\times10^{11}(cm^{-3})$
N_e	[1, 76]	$10^5(cm^{-3})$	$1.3\times10^5(cm^{-3})$	$1.5\times10^5(cm^{-3})$
T_e	[1, 76]	200(k)	400(k)	500(k)
T_i	[1, 76]	200(k)	400(k)	500(k)
T_d	[1, 76]	200(k)	400(k)	500(k)
ω_{pe}	$\omega_{pe}=\sqrt{n_e e^2/\varepsilon_0 m_e}$	$10^7(s^{-1})$	$2\times10^7(s^{-1})$	$2.2\times10^7(s^{-1})$
ω_{pi}	$\omega_{pi}=\sqrt{n_i e^2/\varepsilon_0 m_i}$	$10^4(s^{-1})$	$8.4\times10^4(s^{-1})$	$9.2\times10^4(s^{-1})$
ν_{en}	$\nu_{en}\simeq5.4\times10^{-10}N_nT_e^{1/2}$	$8\times10^4(s^{-1})$	$8.4\times10^3(s^{-1})$	$3.4\times10^3(s^{-1})$
ν_{in}	$\nu_{in}\simeq2.6\times10^{-9}N_n\mu^{-1/2}$	$2\times10^4(s^{-1})$	$406(s^{-1})$	$132(s^{-1})$
B	[77]	0.5(Gauss)	0.5(Gauss)	0.5(Gauss)
Ω_e	$\Omega_e\approx\lvert eB/m_e\rvert$	$10^7(s^{-1})$	$10^7(s^{-1})$	$10^7(s^{-1})$
m_i	[77]	$5\times10^{-23}(gm)$	$5\times10^{-23}(gm)$	$5\times10^{-23}(gm)$
Ω_i	$\Omega_i\approx\lvert eB/m_i\rvert$	$160(s^{-1})$	$160(s^{-1})$	$160(s^{-1})$
c_e	$c_e\approx\sqrt{k_BT_e/m_e}$	$5\times10^6(cms^{-1})$	$7.8\times10^6(cms^{-1})$	$8.7\times10^6(cms^{-1})$
c_i	$c_i\approx\sqrt{k_BT_i/m_i}$	$2.4\times10^4(cms^{-1})$	$3.2\times10^4(cms^{-1})$	$3.6\times10^4(cms^{-1})$
c_d	$c_d\approx\sqrt{k_BT_d/m_d}$	$7.4(cms^{-1})$	$10(cms^{-1})$	$11(cms^{-1})$
m_d	[59, 61]	$5\times10^{-16}(gm)$	$5\times10^{-16}(gm)$	$5\times10^{-16}(gm)$
ν_{dn}	$(m_n/m_d)n_n\langle\sigma v\rangle_{dn}$ [78]	$10(s^{-1})$	$1.3(s^{-1})$	$0.5(s^{-1})$
N_d	[28, 51, 59, 61, 68, 69]	$3\times10^3(cm^{-3})$	$3\times10^3(cm^{-3})$	$3\times10^3(cm^{-3})$

interesting to study the effect of dust size variation on the low frequency hall instability. Below are the results of the effect of dust size variation on the instability in the EEJ region, where the electrons are magnetized, ions and dust particles are unmagnetized. The effect of dust size variation above the EEJ region(∼115 km-∼120 km, ∼125 km-∼130 km) is also studied later in which electrons are strongly magnetized, ions are weakly magnetized and dust particles are unmagnetized. The parameter values typical to the regions are given in table 1.

3. Effect of dusty plasma parameters on hall current instability

3.1. Effect of power law dust size distribution

3.1.1. In the EEJ region (∼95 km − ∼ 105 km)

First we assume a uniform dust size of 50 nm which can be formed due to meteoric ablation, accretion and coagulation processes as reported in [51] and this value was also used by Rosenberg and Shukla [61] in their numerical study of low frequency Hall current instability using kinetic theory.

The dust charge can be estimated from the following formula, $Z_d=\frac{4\pi\epsilon_0 V_0 r_d}{e}$, where ν_0 is the dust surface potential and r_d is the dust radius. By assuming $r_d\sim5\times10^{-8}\ m$ and $\nu_0\sim0.5\ V$, we get $Z_d\approx17$, and the dust plasma frequency becomes, $\omega_{pd}\sim70\ s^{-1}$ for the equilibrium dust number density, $3\times10^3\ cm^{-3}$(see table 1). Now, we consider two types of dust size distribution, one is the narrow size distribution (40 nm − 60 nm) and the other is broad dust size distribution (1 nm − 100 nm). From equation (36), by assuming the value of $\beta\approx3$, $\rho_d\approx1\ gm\ cm^{-3}$ and substituting the value of K from equation (3), we get $\omega_{pd}\sim73\ s^{-1}$ for the narrow dust size distribution and for the broad dust size distribution, we get $\omega_{pd}\sim407\ s^{-1}$. It has been assumed that the dust charged state (Z_d) is approximately constant. We now compare the growth rate (γ_r) and the frequency (ω_r) with the electron drift velocity, V_{e0} in the EEJ region.

Figures 3(a) and (b) show the variation of γ_r and ω_r with the V_{e0} for $k=0.1\ m^{-1}$. From the figures, we can see that γ_r and ω_r increase with the increase of dust size variation and the increase is more significant for the broad dust size distribution in which the growth rate varies from $4\times10^{-4}\ s^{-1}$ to $8.65\ s^{-1}$ and frequency varies from $0.34\ s^{-1}$ to $22\ s^{-1}$ in the range of V_{e0} considered here ($10\ m\ s^{-1}$–$1200 m\ s^{-1}$). For the case of uniform dust size 50 nm, the range of growth rate varies from $9\times10^{-4}\ s^{-1}$ to $0.45\ s^{-1}$ and the frequency varies from $0.12\ s^{-1}$ to $13.6\ s^{-1}$. The growth rate and frequency for narrow dust size distribution varies from $10^{-3}s^{-1}$ to $0.49\ s^{-1}$ and $0.12\ s^{-1}$ to $13.72\ s^{-1}$ respectively. Similar effect is observed in figures 4(a) and (b) which is for $k=0.01\ m^{-1}$ and the other parameters are the same as in figure 3. Therefore, we can conclude that if we consider dust size variation, it can significantly influence the instability.

Figures 5(a) and (b) show the variations of γ_r and ω_r with k for $V_{e0}=720\ m\ s^{-1}$. Here, it can be seen that growth rate and frequency increase with the increase of dust size variation and the increase is much higher for

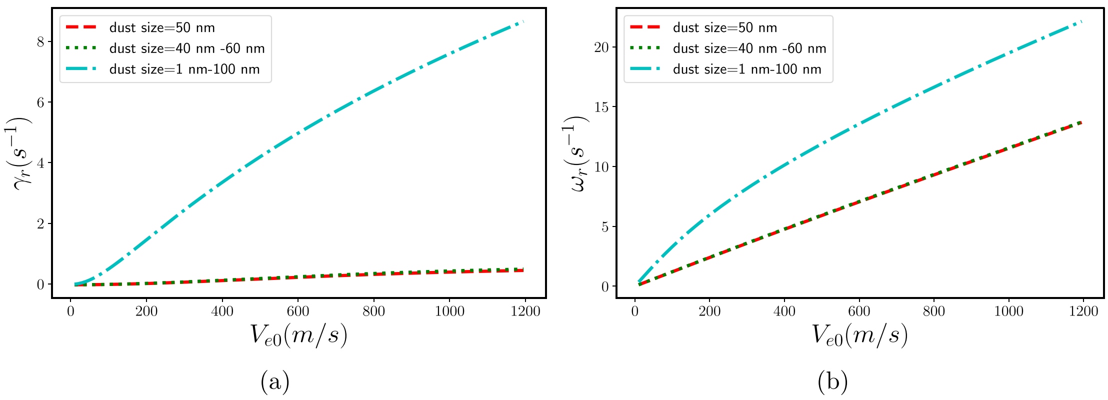

Figure 3. (a) The variation of growth rate, γ_r, with electron drift velocity, V_{e0}, (b) The variation of frequency, ω_r, with electron drift velocity, V_{e0}, for $k = 0.1\ m^{-1}$ in the EEJ region.

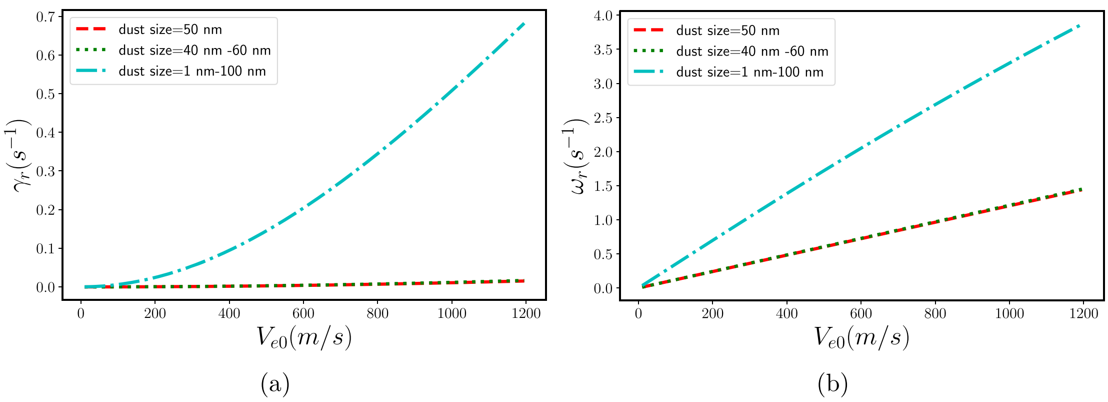

Figure 4. (a) The variation of growth rate, γ_r, with electron drift velocity, V_{e0}, (b) The variation of frequency, ω_r, with electron drift velocity, V_{e0}, for $k = 0.01\ m^{-1}$ in the EEJ region.

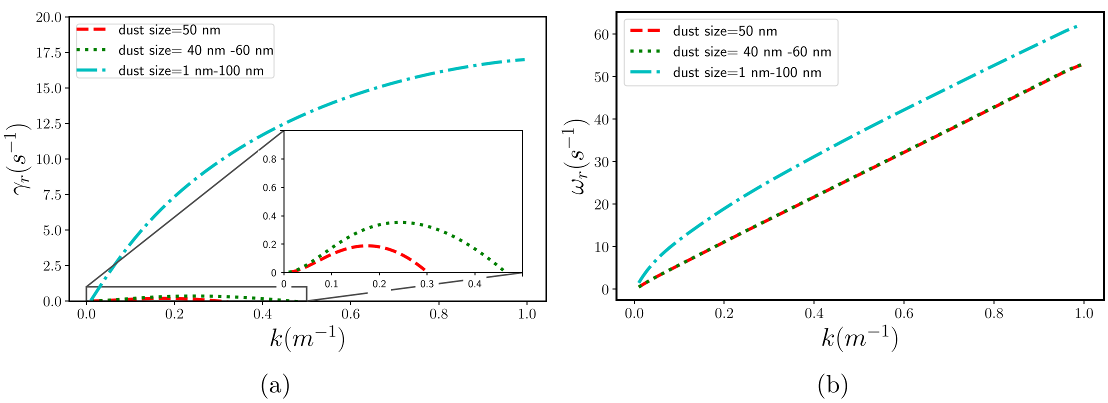

Figure 5. (a) The variation of growth rate, γ_r, with the wave number, k, (b) The variation of frequency, ω_r, with the wave number, *k* for $V_{e0} = 720\ m\ s^{-1}$ in the EEJ region.

broad dust size distribution. In this case, the growth rate varies from 0.13 s^{-1} to 17 s^{-1} while the frequency varies from 1.6 s^{-1} to 62 s^{-1} for the range of k considered here (0.01m^{-1}- 1m^{-1}). However, for the case of uniform dust size and narrow dust size distribution, the growth rate first increases and then decreases. The growth rate and frequency for uniform dust varies from $2 \times 10^{-3}\ s^{-1}$ to $6 \times 10^{-2}\ s^{-1}$ and 0.58 s^{-1} to 52 s^{-1} respectively. And for the case of narrow dust size distribution, the growth rate and frequency vary in the range of $3 \times 10^{-3}\ s^{-1}$ to $2 \times 10^{-2}\ s^{-1}$ and 0.58 s^{-1} to 53 s^{-1} respectively. It is also observed that wave damping(i.e. negative growth

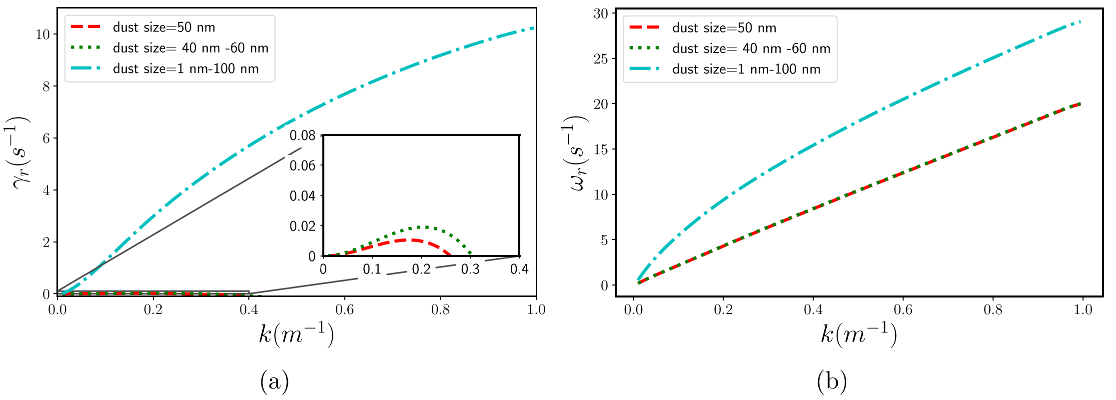

Figure 6. (a) The variation of growth rate, γ_r, with the wave number, k, (b) The variation of frequency, ω_r, with the wave number, k for $V_{e0} = 180\ m\ s^{-1}$ in the EEJ region.

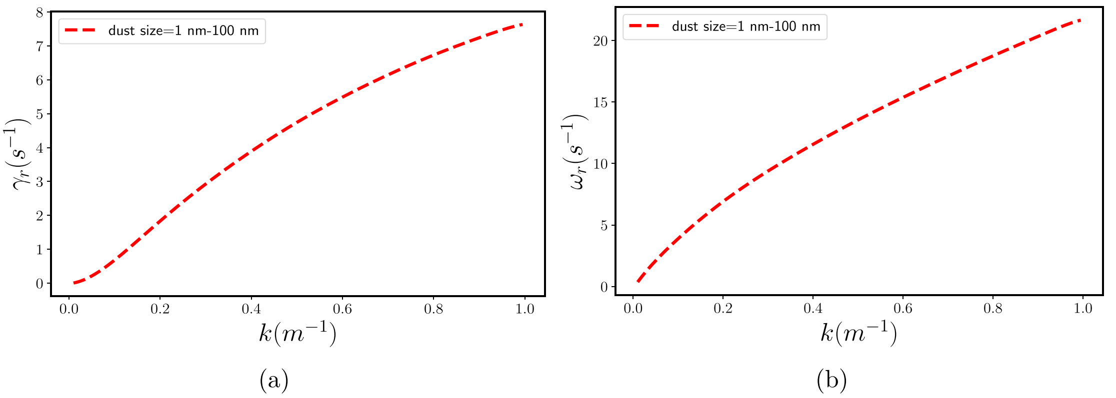

Figure 7. (a) The variation of growth rate, γ_r, with the wave number, k, (b) The variation of frequency, ω_r, with the wave number, k for $V_{e0} = 120\ m\ s^{-1}$ for broad dust size distribution in the EEJ region.

rate)starts at $k = 0.3\ m^{-1}$ for uniform size dust whereas for narrow dust size distribution wave damping starts at $k = 0.45\ m^{-1}$.

Similarly, figures 6(a) and (b) depicted the variation of γ_r and ω_r with k for $V_{e0} = 180\ m\ s^{-1}$. Here, wave damping starts at a lower value of k ($0.27\ m^{-1}$ for uniform size dust and $0.31\ m^{-1}$ for narrow size dust distribution) compare to figure 5 which is expected due to lower electron drift velocity. However, in the case of broad dust size distribution, wave damping mode does not occur for the range of k values considered here. Also, it can be seen that even if the electron drift velocity, V_{e0}($180\ m\ s^{-1}$ in figure 6) is less than the ion thermal velocity (c_i=$240\ m\ s^{-1}$), the instability is excited.

Figures 7(a) and (b) show γ_r and ω_r versus k for $V_{e0} = 120\ m\ s^{-1}$ in the case of broad dust size distribution. The growth rate and frequency vary in the range of $9 \times 10^{-3}\ s^{-1}$ to $7.6\ s^{-1}$ and $0.4\ s^{-1}$ to $21.6\ s^{-1}$ respectively. But, for the case of narrow dust size distribution, we get decaying or wave damping mode (Figure 8(a)) and frequency varies from $0.14\ s^{-1}$ to $13.4\ s^{-1}$(figure 8(b)). Similarly, a decaying mode is also observed for uniform size dust. Therefore, it can be concluded that dust size distribution can significantly alter the required threshold electron drift velocity to excite the instability. The threshold electric field for the instability depends on electron drift velocity and can be estimated from the equation (10) which is found to be few ~mv/m in the EEJ region.

3.1.2. Above the electrojet region

(a) Altitude range (~115 km — ~ 120km)

The above mode analysis is for the EEJ region in which $\Omega_i \ll \nu_{in}$. Since ions are unmagnetized in the EEJ region, the ion's drift has been neglected. However, above the EEJ region(~115 km–~120 km), ν_{in} decreases due to lower neutral density and becomes roughly comparable or in the same order as Ω_i. Therefore, ions become weakly magnetized and the ion's drift can no longer be neglected. To understand the effect of weakly magnetized

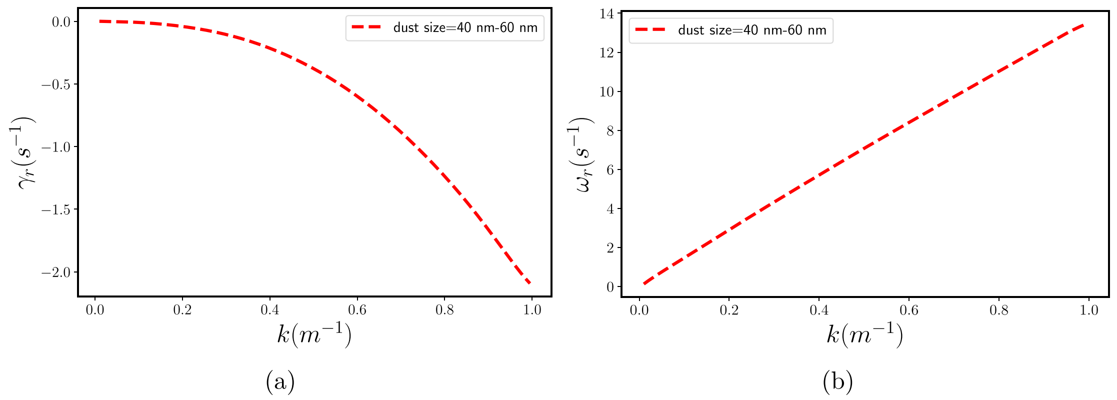

Figure 8. (a) The variation of growth rate, γ_r, with the wave number, k, (b) The variation of frequency, ω_r, with the wave number, k for $V_{e0} = 120$ m s^{-1} for narrow dust size distribution in the EEJ region.

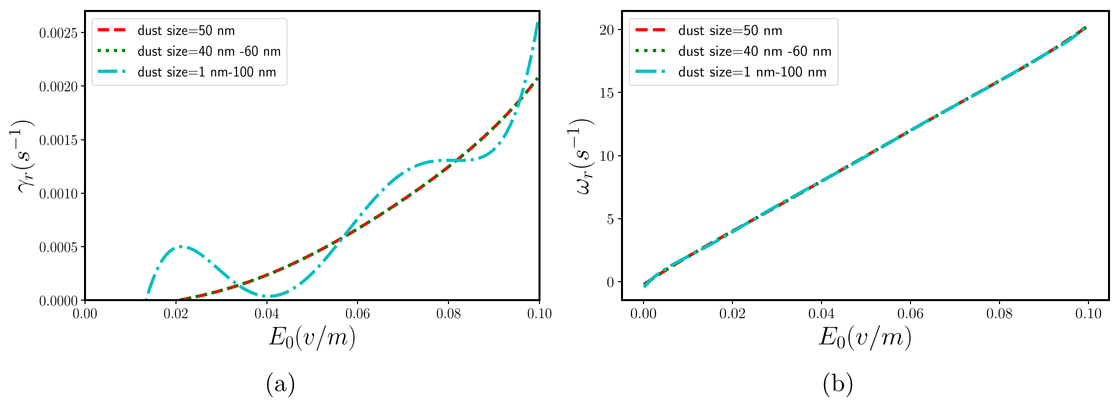

Figure 9. (a)The variation of growth rate, γ_r, with the electric field, E_0, (b) The variation of frequency, ω_r, with the electric field, E_0 for $k = 0.01$ m^{-1} in the region (~115 km − ~ 120 km).

ions on the instability, the dispersion relation (equation (33)) is solved for the parameters of the altitude range ~115 km–~120 km.

The electron and ion drifts in the y direction can be calculated from equation (10). These are, $|V_{e0y}| \sim 2 \times 10^4 E_0$ m s^{-1} and $|V_{i0y}| \sim 3 \times 10^3 E_0$ m s^{-1} in which, E_0 is the magnitude of the equilibrium electric field. Since the value of E_0 can be as low as in the order of few mv for the excitation of the instability, the range of E_0 is taken from 10^{-4} v m^{-1} to 10^{-1} v m^{-1}.

Figures 9(a) and (b) show the variation of γ_r and ω_r with E_0 for uniform as well as variable size dust particles for $k = 0.01$ m^{-1}. It can be seen that the growth rate and frequency decreases compared to the EEJ region due to the lower neutral density. Also, it is found that growth rate and frequency do not increase with the dust size variation which is not the case in the EEJ region. Moreover, for broad dust size distribution, although the threshold electric field for the instability can be slightly lower compared to the other dust sizes, the growth rate is oscillating.

Figures 10(a) and (b) are similar as figure 9(a) and (b) but for $k = 0.1$ m^{-1}. The γ_r and ω_r increases compare to figures 9(a) and (b) due to higher values of k. However, the variation of dust size cannot increase the γ_r and ω_r which is also observed for $k = 0.01$ m^{-1}. Figures 11(a) and (b) show the variation of γ_r and ω_r with k for $E_0 = 10$ mV m^{-1} for different dust size distribution. Here, also it can be seen that variation of dust size cannot alter the γ_r and ω_r of the instability.

(b) Altitude Range (~125 km − ~ 130 km)

Again, the dispersion relation is solved for above the EEJ region for the altitude range of ~125 km - ~130 km. In this region ion neutral collision frequency, ν_{in} is lower than ion gyro-frequency, Ω_i. Figures 12 and 13 show γ_r and ω_r variation with E_0 for the different dust sizes for $k = 0.01$ m^{-1} and $k = 0.1$ m^{-1} respectively. From figure 12(a), it can be seen that the mode is damped whereas a positive growth rate was obtained for the same value of k (0.01m^{-1}) in the region(~115 km - ~120 km)(see figure 9(a)). For $k = 0.1$ m^{-1} in figure 13(a),

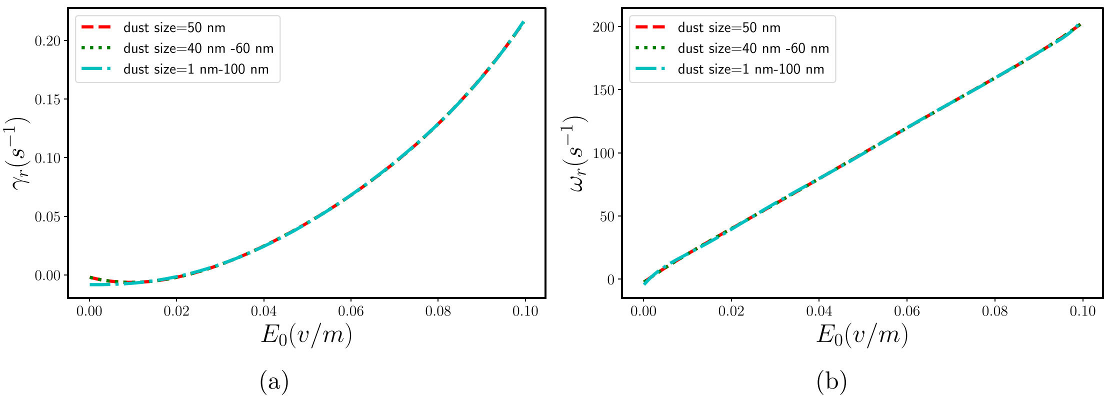

Figure 10. (a) The variation of growth rate, γ_r, with the electric field, E_0, (b) The variation of frequency, ω_r, with the electric field, E_0 for $k = 0.1\ m^{-1}$ in the region (~115 km – ~ 120 km).

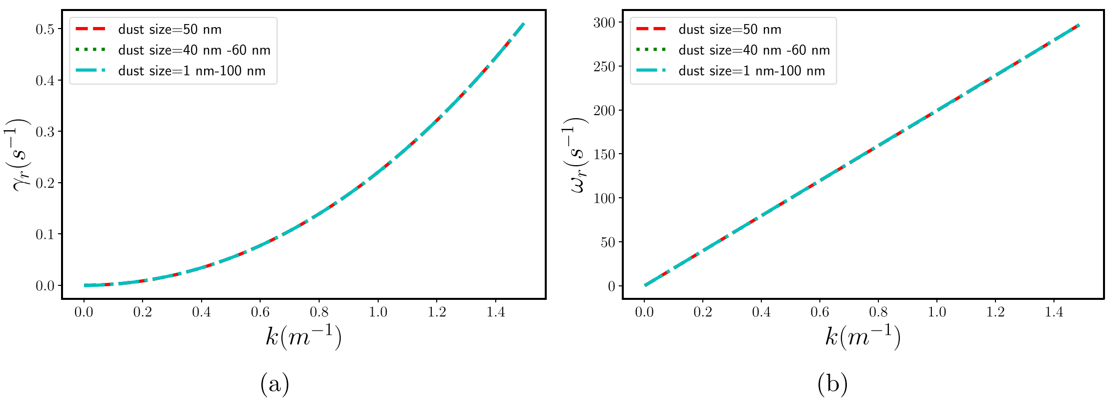

Figure 11. (a)The variation of growth rate, γ_r, with the wave number, k, (b) The variation of frequency, ω_r,with the wave number, k, for $E_0 = 10$ mV m^{-1} in the region (~115 km – ~ 120 km).

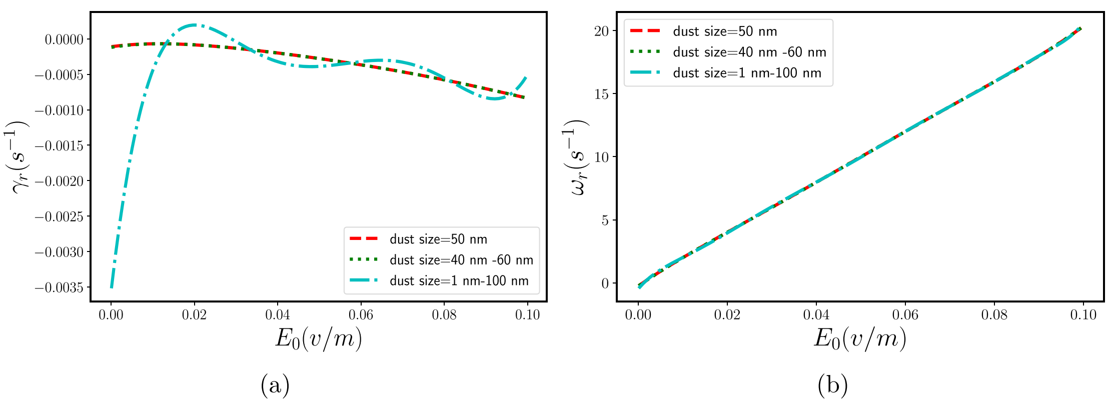

Figure 12. (a) The variation of growth rate, γ_r, with the electric field, E_0, (b) The variation of frequency, ω_r, with the electric field, E_0 for $k = 0.01\ m^{-1}$ in the region (~125 km – ~ 130 km).

although the wave has a positive growth rate but decreases compared to the figure 10(a). Figures 14(a) and (b) represent the variation of γ_r and ω_r with k for $E_0 = 10$ mV m^{-1}. The value of γ_r and ω_r is slightly decreased compared to the case (a) (figures 11(a) and (b)). Also, in this region effect of dust size variation cannot alter the growth rate and frequency of the instability which is as similar as observed in the previous case. Therefore, it can be concluded that when ions become weakly magnetized, the dust size variation can not significantly affect the growth rate and frequency of the instability.

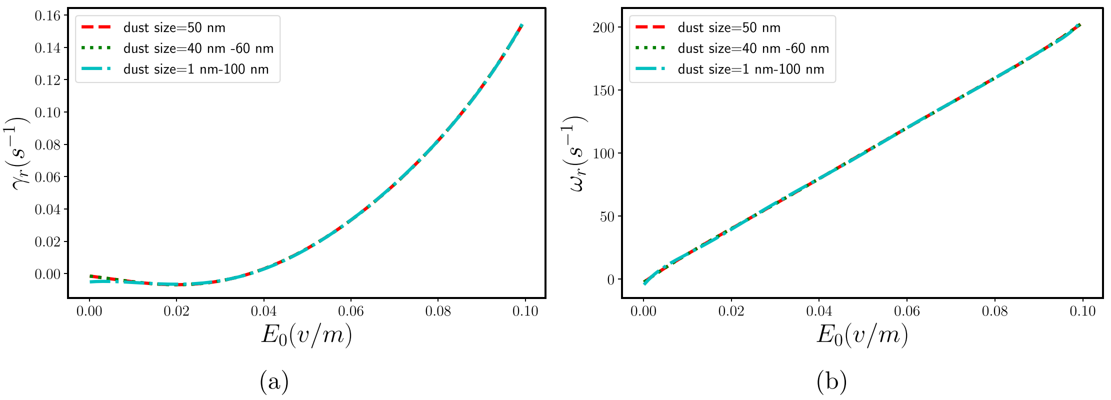

Figure 13. (a) The variation of growth rate, γ_r, with the electric field, E_0, (b) The variation of frequency, ω_r, with the electric field, E_0 for $k = 0.1\ m^{-1}$ in the region (∼125 km − ∼ 130 km).

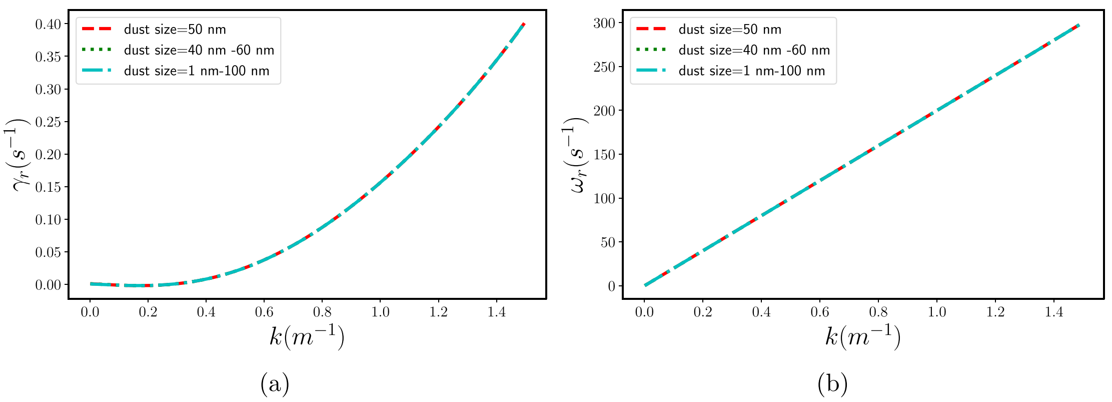

Figure 14. (a) The variation of growth rate, γ_r, with the wave number, k, (b) The variation of frequency, ω_r, with the wave number, k, for $E_0 = 10\ mV\ m^{-1}$ in the region (∼125 km − ∼ 130 km).

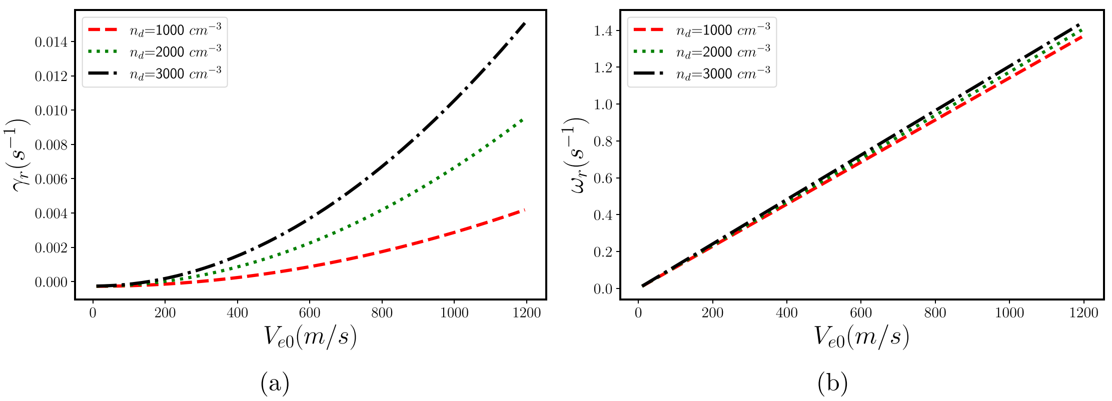

Figure 15. (a) The variation of growth rate, γ_r, with electron drift velocity, V_{e0}, (b) The variation of frequency, ω_r, with electron drift velocity, V_{e0} for different dust densities in the EEJ region for $k = 0.01\ m^{-1}$.

3.2. Effect of dust number density

As discussed in the introduction, the dust number density can vary in the region of interest due to complex dust forming processes and exists upto altitudes of 130 km [62]. Figures 15(a) and (b) show the plot of the growth rate, γ_r and frequency,ω_r with electron drift velocity, V_{e0} for the case of uniform size dust having three different dust densities in the EEJ region. It is discernible that γ_r and ω_r of the instability increases with the increase of n_d. However, in the altitude range (∼115 km - ∼120 km) and (∼125 km - ∼130 km), the variation of dust number

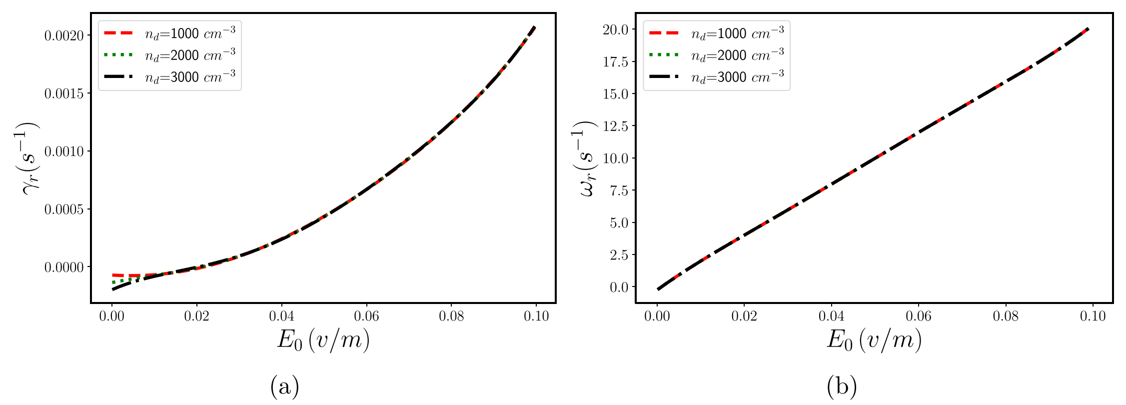

Figure 16. (a) The variation of growth rate, γ_r, with the electric field, E_0, (b) The variation of frequency, ω_r, with the electric field, E_0 for different dust densities in the region (∼115 km − ∼ 120 km) for $k = 0.01\ m^{-1}$.

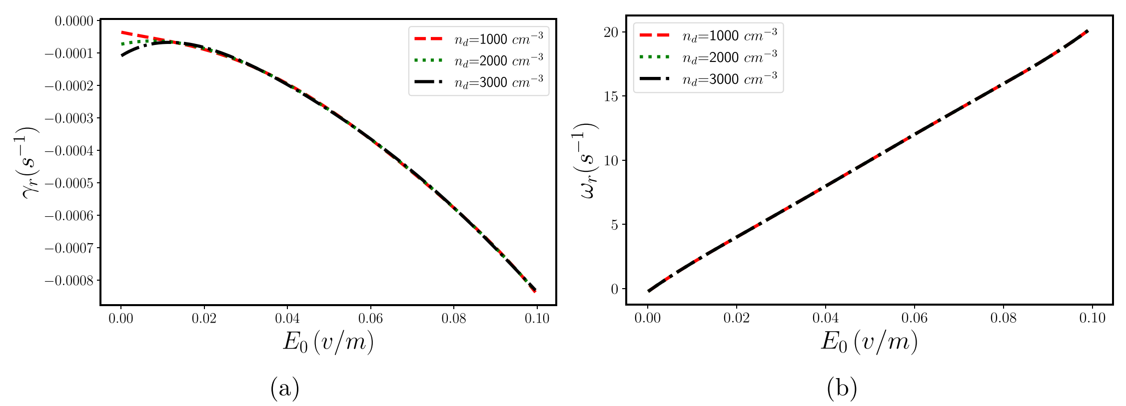

Figure 17. (a) The variation of growth rate, γ_r, with the electric field, E_0, (b) The variation of frequency, ω_r, with the electric field, E_0 for different dust densities in the region (∼125 km − ∼ 130 km) for $k = 0.01\ m^{-1}$.

densities cannot affect the instability (see figure 16 and figure 17) as similar as observed for the case of dust size variation in these regions.

4. Analytical result in the electrojet region

Since electrons are magnetized, it can be assumed that $\Omega_e \gg \nu_{en}$. Then the equation (27) for the electron susceptibilty, χ_e takes the following form:

$$\chi_e = \frac{\omega_{pe}^2(\omega - k_y V_{e0} + i\nu_{en})}{\Omega_e^2[(\omega - k_y V_{e0}) + (\omega - k_y V_{e0} + i\nu_{en})k^2\rho_e^2]}, \tag{41}$$

where, $\rho_e = \frac{c_e}{\Omega_e}$ is the electron gyroradius.

For the case of ions, let's consider $(\omega + i\nu_{in}) \ll kc_i$ [61] and also neglecting the ion-drift, V_{ioy} in equation (28), so that the ion susceptibility, χ_i becomes,

$$\chi_i \approx \frac{1}{k^2\lambda_{Di}^2}. \tag{42}$$

Since, dust is also unmagnetized, let's assume $\Omega_d \approx 0$ and $V_{d0y} \approx 0$. Also, by neglecting the dust thermal velocity, c_d, the equation (29) for dust susceptibility becomes,

$$\chi_d \approx -\frac{\omega_{pd}^2}{\omega(\omega + i\nu_{dn})}, \tag{43}$$

now, considering weak collision ($\nu_{\mathrm{dn}} \ll \omega$), the above equation can also be written as,

$$\chi_{\mathrm{d}} \approx -\frac{\omega_{\mathrm{pd}}^2}{\omega^2}\left(1 - i\frac{\nu_{\mathrm{dn}}}{\omega}\right). \tag{44}$$

The approximate dispersion relation then takes the following form,

$$1 + \frac{\omega_{\mathrm{pe}}^2(\omega - \mathrm{k_y V_{e0}} + \mathrm{i}\nu_{\mathrm{en}})}{\Omega_{\mathrm{e}}^2[(\omega - \mathrm{k_y V_{e0}}) + (\omega - \mathrm{k_y V_{e0}} + \mathrm{i}\nu_{\mathrm{en}})\mathrm{k}^2\rho_{\mathrm{e}}^2]} + \frac{1}{\mathrm{k}^2\lambda_{\mathrm{Di}}^2} - \frac{\omega_{\mathrm{pd}}^2}{\omega^2}\left(1 - \mathrm{i}\frac{\nu_{\mathrm{dn}}}{\omega}\right) = 0. \tag{45}$$

Since ω is complex, assume $\omega = \omega_{\mathrm{r}} + \mathrm{i}\gamma_{\mathrm{r}}$ and also let's consider a weak growth rate, $|\gamma_{\mathrm{r}}| \ll \omega_{\mathrm{r}}$. Then the real part of the dispersion relation(equation (45)) gives,

$$\frac{\omega_{\mathrm{r}}^2}{\omega_{\mathrm{pd}}^2(1 + \mathrm{k}^2\rho_{\mathrm{e}}^2)} \approx \frac{\mathrm{k}^2\lambda_{\mathrm{Di}}^2\Omega_{\mathrm{e}}^2}{\Omega_{\mathrm{e}}^2(1 + \mathrm{k}^2\rho_{\mathrm{e}}^2)(1 + \mathrm{k}^2\lambda_{\mathrm{Di}}^2) + \omega_{\mathrm{pe}}^2\mathrm{k}^2\lambda_{\mathrm{Di}}^2}. \tag{46}$$

For long wave length limit, $\mathrm{k}^2\rho_{\mathrm{e}}^2 \ll 1$, then the above equation reduces to,

$$\omega_{\mathrm{r}}^2 \approx \frac{\mathrm{k}^2\lambda_{\mathrm{Di}}^2\omega_{\mathrm{pd}}^2}{1 + \mathrm{k}^2\lambda_{\mathrm{Di}}^2\left(1 + \frac{\omega_{\mathrm{pe}}^2}{\Omega_{\mathrm{e}}^2}\right)}. \tag{47}$$

Now, from the imaginary part of the equation (45), for weak growth rate,

$$\gamma_{\mathrm{r}} = \frac{D_i(\omega, \mathrm{k})}{\frac{\partial D}{\partial \omega}\Big|_{\gamma=0}}, \tag{48}$$

again, considering the long wave length limit, $\mathrm{k}^2\rho_{\mathrm{e}}^2 \ll 1$, we get,

$$\frac{\partial D}{\partial \omega}\Big|_{\gamma=0} = -\frac{2\omega_{\mathrm{pd}}^2}{\omega_{\mathrm{r}}^3}. \tag{49}$$

Finally, we obtain the following approximate form for the weak growth rate,

$$\frac{\gamma_{\mathrm{r}}}{\omega_{\mathrm{r}}} = \frac{\omega_{\mathrm{r}}^2}{2\omega_{\mathrm{pd}}^2}\left(\frac{\omega_{\mathrm{pe}}}{\Omega_e}\right)^2\frac{\nu_{\mathrm{en}}}{\mathrm{kV_{eo}} - \omega_{\mathrm{r}}} - \frac{\nu_{\mathrm{dn}}}{2\omega_{\mathrm{r}}}. \tag{50}$$

5. Discussion

Let us first discuss the physical implication of the mathematical analysis carried out in this work. The obtained general dispersion relation (equation (33)) consists of all the charged species inertia, thermal velocity, drift velocity, Langmuir and gyrofrequency. This unified treatment allows us to study from the condition in which only electrons are magnetized (in the EEJ region) to a condition in which both electrons and ions are magnetized but the dust particles are unmagnetized (above the EEJ region).

Following the mathematical analysis, the physical condition for the instability excitation can be understood as follows: The electric field, $\mathbf{E}_0$(which is perpendicular to the geomagnetic field, $\mathbf{B}$) drives the electrons with the drift velocity $\mathbf{V}_{e0}$(equations (9) and 10). Since electron-neutral collision frequency, ν_{en} is approximately two or three tenths of magnitudes lesser than electron gyrofrequency, Ω_{e}, both in the EEJ or above the EEJ region(see table 1), then from equations (9) and (10),$\mathbf{V}_{e0y} \gg \mathbf{V}_{e0x}$. The magnitude of the V_{e0y} can be approximated as $\sim\mathrm{E}_0/B$. On the other hand, ion and dust drift $\mathbf{V}_{i0}$ and $\mathbf{V}_{d0}$ is much lesser than $\mathbf{V}_{e0}$ in the EEJ region such that ion and dust drift can be neglected in the EEJ region. However, above the EEJ region, non-negligible finite ion drift exists owing to the fact that ν_{in} becomes comparable to Ω_{i}. The large relative drift between electrons, ions and dust generate a Hall current which may excite instabilities in and above the EEJ region. The wave vector $\mathbf{k}$ of the electrostatic waves arises due to the instabilities are mostly in the perpendicular direction of the magnetic field, $\mathbf{B}$ and the frequencies in the range of dust-acoustic frequency which is much lower than electron gyro frequency, Ω_{e} but much higher than the dust gyrofrequency, Ω_{d}.

The analytical expression for the frequency(ω_{r}) and the growth rate (γ_{r}) derived here using a fluid model in the long wavelength and weak collisional limit is fully consistent with the results obtained by Rosenberg and Shukla [61] using kinetic theory. From equation (50), it can be seen that instability develops if electron drift speed is larger than the phase speed of dust acoustic waves. Also, it shows that the growth rate,γ_{r}, is proportional to the electron-neutral collision frequency, ν_{en}. Since ν_{en} varies from $\sim10^4\ \mathrm{s}^{-1}$ to $\sim10^3\ \mathrm{s}^{-1}$ in the EEJ region, γ_{r} and ω_{r} decrease with altitude which is also evident from the numerical analysis presented in section-2. In addition, dust-neutral collision frequency, ν_{dn} further reduces the growth rate as can be seen from equation (50). However, in the upper EEJ region the damping due to ν_{dn} is small due to lower neutral densities. Moreover,γ_{r}

and ω_r are proportional to ω_{pd}. Since ω_{pd} significantly increases for broad dust size distribution and higher dust number density, the instability is more easily excited in these cases which further validates the numerical analysis presented for the EEJ region.

Also, Rosenberg and Shukla [61] showed that in the EEJ altitude the instability criteria is more easily satisfied by the dust particles which are charged positively due to photoemission by solar UV radiation. Now, if the dust particles emit photoelectrons with much higher energies than the ambient electrons, it can enhance the electron temperature which leads to the higher electron density due to the reduction of electron-ion recombination coefficient [73]. Therefore, in this case, ν_{en} may increase which can further increase the γ_r and ω_r.

Now, above the EEJ region, ν_{dn} decreases considerably (see table 1). Since dust particles are unmagnetized (in the entire altitude range), so dust cross-field drift can be neglected. Therefore, dust susceptibility, χ_d for above the EEJ region can still be expressed by equation (43). However, since ν_{dn} is much smaller than that of the EEJ region, it can be neglected. On the other hand, since the ion susceptibility, χ_i contains ion drift term, ion contribution dominates in the wave motion. Since the variation in the dust size and number density, both are related to the parameter ω_{pd}, the variation of ω_{pd} has negligible effect on the growth rate and frequency of the wave which is evident from the numerical analysis presented above the EEJ region.

Finally, we discuss the role and the consequence of the underlying physical assumptions.

(i) Equilibrium plasma density gradients which have been neglected in this work may have a considerable effect on the instability. By, using kinetic theory, it has been shown that the presence of a small equilibrium electron density gradient scale length due to the short-scale variation of dust charge density can substantially increase the growth rate of the instability [60]. In this case, the negatively charged dust modifies the phase speed of the waves via its effect on equilibrium charge neutrality. Moreover, by considering dust dynamics, low frequency gradient drift instability or dust acoustic drift wave instability for uniform size positively charged dust grains have been investigated [74]. It has been shown that sufficient density of positively charged dust in the meteor trail plasma, can excite the instability which is driven by the electron diamagnetic and cross field drift whose magnitude is smaller than the ion thermal speed [74]. Therefore, our model which includes the variable size dust grain can be extended for the case of low frequency gradient drift instability.

(ii) The previous study by Fejer *et al* [70] shows (without taking into consideration of dust fluid) that electron-ion recombinational damping can substantially increase the threshold drift velocity for the marginal instability of the two-stream ion-cyclotron waves in the auroral E-region. It has been shown that the the recombinational effect is important even for the case of short wavelengths (10–20 m) at altitudes where the ion-neutral collision frequency is comparable to the ion gyro frequency. Therefore, we believe that the case of electron-ion recombination at the dust particle's surface may alter the threshold condition of the low frequency hall current instability and can be studied in detail.

(iii)
In the present analysis wave propagation parallel to the magnetic field, B has not been considered. It has been shown that parallel propagation can slightly shift the unstable wavelength to longer wavelength and under certain conditions maximum growth rate can be obtained for slightly off-angle propagation [75]. So, it is interesting to investigate the effect of parallel propagation on the instability for the case variable size dust grain.

Last but not the least, various other assumptions like electron-ion collision, equilibrium temperature gradient, neutral wind velocity and so on, may also influence the instability and can be studied subsequently.

6. Conclusion

Low frequency hall current instabilities have been investigated in and above the electrojet region using a fluid model for three charged components (electrons, ions and dust particles). At the EEJ altitude, only the electrons are strongly magnetized and the other two components are unmagnetized. But above the EEJ altitude electrons are strongly magnetized, ions are weakly magnetized and dust particles are unmagnetized. The perturbed electron, ion and dust densities have been obtained after linearizing the continuity and momentum equations. Then the dispersion relation is obtained through linearizing Poission's equation. The effect of power-law dust size variation and dust number density on the instability has been studied in detail. The variation in the growth rate and frequency of the instability (for uniform dust size as well as variable dust size) (a) with electron drift speed for two different values of wave number and (b) with wave number for three fixed values of electron drift speed have been shown in the EEJ region. In this region, the instability is excited even if the electron drift speed smaller than the ion thermal speed and the variation of dust size and dust number density have significant effects on the instability. However, above the EEJ region, the growth rate and frequency of the wave decreases compare to the EEJ region. Also, dust size variation and dust number density do not affect the instability above the EEJ altitudes. Since it has been shown that variable size charged dust particles which are formed due to the meteoric ablation can affect the Hall current instability, the present work finds application in those regions of the lower ionosphere where meteor trail plasma forms.

In this work, the equilibrium plasma density and temperature gradient, recombination of electron-ion on the dust particle's surface, the effect of electron-ion collision, neutral wind velocity, the effect of parallel propagation and the electric field shear effects have been neglected in the model. The limitation of the model also includes the dust mass density (ρ_d) and surface potential(v_0) which are approximately constant and the same for all dust particle sizes. Considering these predefined approximations in the future model will certainly improve the dusty electrojet model and make it more realistic typical to the E-region ionosphere perturbed by meteoric ablation phenomenon.

During geomagnetic disturb conditions, the electric field of the equatorial electrojet ionosphere can be substantially perturbed by the magnetospheric convection electric field (also called direct prompt penetration electric field) [79] and ionospheric disturbance dynamo [80]. The effect of a non-uniform electric field (transverse to the uniform magnetic field in inhomogeneous ionospheric plasma) on the dusty drift waves and instabilities can be studied. Also, enhanced fluctuations occur during strong auroral activities in the polar E-region of the ionosphere in the region of equilibrium plasma density and temperature gradients [81]. The coupling of the low frequency dust waves with the plasma inhomogeneity in variable size dusty plasma may also be considered in the future work.

Acknowledgments

One of the author(Jyoti K Atul) acknowledges Prof. Prabal K. Chattopadhyay of Institute for Plasma Research, Gandhinagar, India and Prof. S. Sripathi of Indian Institute of Geomagnetism, Navi Mumbai, India for useful discussion. We thank anonymous referees for useful suggestions which help to improve the manuscript.

Data availability statement

All data that support the findings of this study are included within the article (and any supplementary files).

ORCID iDs

Sanjib Sarkar https://orcid.org/0000-0003-2636-514X
Jyoti K Atul https://orcid.org/0000-0002-6994-2712
Modhuchandra Laishram https://orcid.org/0000-0002-8644-1434

References

[1] Kelley M C 2009 *The Earth's ionosphere: Plasma physics and electrodynamics* (Academic Press)
[2] Sudan R N 1983 Unified theory of Type I and Type II irregularities in the equatorial electrojet *J. Geophys. Res.* **88** 4853–60
[3] Atul J K, Sarkar S and Singh S K 2016 Nonlinearly coupled dynamics of irregularities in the equatorial electrojet *Phys. Lett.* A **380** 1446–9
[4] Farley D T 1963 A plasma instability resulting in field-aligned irregularities in the ionosphere *J. Geophys. Res.* **68** 6083–97
[5] Buneman O 1963 Excitation of field aligned sound waves by electron Stream *Phys. Rev. Lett.* **10** 285
[6] Reid G C 1968 The formation of small-scale irregularities in the ionosphere *J. Geophys. Res.* **73** 1627–40
[7] Bowles K L, Balsley B B and Cohen R 1963 Field aligned E region irregularities identified with acoustic plasma waves *J. Geophys. Res.* **68** 2485–501
[8] Balsley B B 1969 Some characteristics of non-two-stream irregularities in the equatorial electrojet *J. Geophys. Res.* **74** 2333–47
[9] Balsley B B and Farley D T 1971 Radar studies of the equatorial electrojet at three frequencies *J. Geophys. Res.* **76** 8341–51
[10] Fejer B G, Farley D T, Balsley B B and Woodman R F 1975 Oblique VHF radar spectral studies of the equatorial electrojet *J. Geophys. Res.* **80** 1307–12
[11] Fejer B G, Farley D T, Balsley B B and Woodman R F 1976 Radar observations of two-dimensional turbulence in the equatorial electrojet *J. Geophys. Res.* **81** 130–4
[12] Sudan R N, Akinrimisi J and Farley D T 1973 Generation of small-scale irregularities in the equatorial electrojet *J. Geophys. Res.* **78** 240–8
[13] Sharma S K and Kaw P K 1986 Modification of type II irregularities by finite amplitude type I waves in equatorial electrojet *J. Geophys. Res.* **91** 12118–20
[14] Ronchi C, Sudan R N and Similon P L 1990 Effect of short-scale turbulence on kilometer wavelength irregularities in the equatorial electrojet *J. Geophys. Res.* **95** 189–200
[15] Smolyakov A I, Koustov A V and Makarevitch R A 2001 Secondary instabilities in the dynamics of the Farley-Buneman fluctuations *J. Geophys. Res.* **106** 15511–8
[16] Alken P and Maus S 2010 Relationship between the ionospheric eastward electric field and the equatorial electrojet *Geophys. Res. Lett.* **37** L04104

[17] Fang T W, Richmond A D, Liu J Y, Maute A, Lin C H, Chen C H and Harper B 2008 Model simulation of the equatorial electrojet in the Peruvian and Philippine sectors *J. Atmos. Terr. Phys.* **70** 2203–11
[18] Sugiura M and Cain J C 1966 A model equatorial electrojet *J. Geophys. Res.* **71** 1869–77
[19] Sugiura M and Poros D J 1969 An improved model equatorial electrojet with a meridional current system *J. Geophys. Res.* **74** 4025–34
[20] Dimant Y S and Oppenheim M M 2004 Ion thermal effects on E-region instabilities: linear theory *J. Atmos. Sol.-Terr. Phys.* **66** 1639–54
[21] Shukla P K and Mamun A A 2002 *Introduction to Dusty Plasma Physics* (Bristol: IoP Publisher) 270
[22] Fortov V E, Ivlev A V, Khrapak S A, Khrapak A G and Morfill G E 2005 Complex (dusty) plasmas: current status, open issues, perspectives *Phys. Rep.* **421** 1–103
[23] Merlino L and Goree J A 2004 Dusty plasmas in the laboratory, industry and space *Phys. Today* 32–8
[24] Zubko V, Dwek E and Arendt R G 2004 Interstellar dust models consistent with extinction, emission, and abundance constraints *Astrophys. J.* **152** 211–49
[25] Pollack J B, Hollenbach D, Beckwith S, Simonelli D P, Roush T and Fong W 1994 Composition and radiative properties of grains in molecular clouds and accretion disks *Astrophys. J.* **421** 615–39
[26] Goertz C K 1989 Dusty plasmas in the solar system *Rev. Geophys.* **27** 271–92
[27] Davies J K, Roush T L, Cruikshank D P, Bartholomew M J, Geballe T R, Owen T and de Bergh C 1997 The detection of water ice in comet Hale-Bopp *Icarus* **127** 238–45
[28] Scales W A and Mahmoudian A 2016 Charged dust phenomena in the near-Earth space environment *Rep. Prog. Phys.* **79** 106802
[29] Mann I *et al* 2011 Dusty plasma effects in near Earth space and interplanetary medium *Space Sci. Rev.* **161** 1–47
[30] Zadorozhny Z M 2001 Effects of charged dust on mesospheric electrical structure *Adv. Space Res.* **28** 1059–64
[31] Havnes O, Troim J, Blix T, Mortensen W, Naesheim L I, Thrane E and Tonnesen T 1996a First detection of charged dust particles in the Earth's mesosphere *J. Geophys. Res.* **101** 10839–47
[32] Havnes O, Naesheim L I, Hartquist T W, Morfill G E, Melandsø F, Schleicher B, Trøim J, Blix T and Thrane E 1996b Meter-scale variation of the charge carried by mesospheric dust *Planet. Space Sci.* **44** 1191–4
[33] Havnes O, Aslaksen T and Brattli A 2001 Charged dust in the Earth's middle atmosphere *Phys. Scr.* **T89** 133–7
[34] Havnes O, La Hoz C, Biebracher A, Kassa M, Meseret T, Naesheim I and Zivkovic T 2004 Investigation of the mesospheric PMSE conditions by use of the new overshoot effect *Phys. Scr.* **T107** 70–8
[35] Havnes O and Kassa M 2009 On the sizes and observable effects of dust particles in polar mesospheric winter echoes *J. Geophys. Res.* **114** D09209
[36] Kulkarni V H and Muralikrishna P 2006 The role of dusts on the equatorial electrojet currents *J. Atmos. Sol.-Terr. Phys.* **68** (2) 228–35
[37] Muralikrishna P and Kulkarni V H 2006 On the height variation of the E-region cowling conductivity - effect of charged dust particles *Ann. Geophys.* **24** 2949–57
[38] Muralikrishna P and Kulkarni V H 2008 Modeling the meteoric dust effect on the equatorial electrojet *Adv. Space Res.* **42** 164–70
[39] Kopnin S I, Popel S I and Yu M Y 2009 Phenomena associated with complex (dusty) plasmas in the ionosphere during high-speed meteor showers *Phys. Plasmas* **16** 063705
[40] Lynch K A, Gelinas L J, Kelley M C, Collins R L, Widholm M, Rau D, Mac Donald E, Liu Y, Ulwick J and Mace P 2005 Multiple sounding rocket observations of charged dust in the polar winter mesosphere *J. Geophys. Res.* **110** A03302
[41] Li Q, Rapp M, Röttger J, Latteck R, Zecha M, Strelnikova I, Baumgarten G, Hervig M, Hall C and Tsutsumi M 2010 Microphysical parameters of mesospheric ice clouds derived from calibrated observations of polar mesosphere summer echoes at Bragg wavelengths of 2.8 m and 30 cm *J. Geophys. Res.* **115** D00I13
[42] Rapp M 2000 Capture rates of electrons and positive ions by mesospheric aerosol particles *J. Aerosol Sci.* **31** 1367–9
[43] Rapp M and Lubken F J 2003 On the nature of PMSE: electron diffusion in the vicinity of charged particles revisited *J. Geophys. Res.* **108** 8437
[44] Rapp M and Lubken F J 2004 Polar mesosphere summer echoes (PMSE): review of observations and current understanding *Atmos. Chem. Phys.* **4** 2601–33
[45] Rapp M and Thomas G E 2006 Modeling the microphysics of mesospheric ice particles: assessment of current capabilities and basic sensitivities *J. Atmos. Sol.-Terr. Phys.* **68** 715–44
[46] Rapp M, Hedin J, Strelnikova I, Friedrich M, Gumbel J and Lübken F-J 2005 Observations of positively charged nanoparticles in the nighttime polar mesosphere *Geophys. Res. Lett.* **32** L23821
[47] Gelinas L J, Lynch K A, Kelley M C, Collins S, Baker S, Zhou Q and Friedman J S 1998 First observation of meteoric charged dust in the tropical mesosphere *Geophys. Res. Lett.* **25** 4047–50
[48] Gelinas L J *et al* 2005 Mesospheric charged dust layer: implication for neutral chemistry *J. Geophys. Res.* **110** A01310
[49] Oppenheim M M, Dyrud L P and Ray L 2003 Plasma instabilities in meteor trails: linear theory *J. Geophys. Res.* **108** A2
[50] Chapin E and Kudeki E 1994a Plasma-wave excitation on meteor trails in the equatorial electrojet *Geophys. Res. Lett.* **21** 2433–6
[51] Kelley M C, Alcala C and Cho J Y N 1998 Detection of a meteor contrail and meteoric dust in the Earth's upper mesosphere *J. Atmos. Sol.-Terr. Phys.* **60** 359–69
[52] Rietmeijer F J M, Nuth J A and Karner J M 1999 Metastable Eutectic Condensation in a Mg-Fe-SiO-$H_2 - O_2$ Vapor: Analogs to Circumstellar Dust *Astrophys. J.* **527** 395–404
[53] Mateshvili N, Mateshvili I, Mateshvili G, Gheondijan L and Kapanadze Z 1998 Dust particles in the atmosphere during the Leonid meteor showers of 1998 and 1999 *Earth Moon Planets* **82-83** 489–504
[54] Rosinski J and Snow R H 1961 Secondary particulate matter from meteor vapors *J. Meteor* **18** 736–45
[55] Hunten D M, Turco R P and Toon O B 1980 Smoke and dust particles of meteoric origin in the mesosphere and stratosphere *J. Atmos. Sci.* **37** 1342–57
[56] Shukla P K and Silin V P 1992 Dust ion-acoustic wave *Phys. Scr.* **45** 508
[57] Rao N N, Shukla P K and Yu M Y 1990 Dust-Acoustic Waves in Dusty Plasmas *Planet. Space Sci.* **38** 543
[58] Barkan A, Merlino R L and D'Angelo N 1995 Laboratory observation of the dust-acoustic wave mode *Phys. Plasmas* **2** 3563
[59] Rosenberg M and Chow V W 1998 Farley-Buneman instability in a dusty plasma *Planet. Space Sci* **46** 103–8
[60] Rosenberg M and Shukla P K 2003 Gradient-drift instability in space dusty plasmas *Planet. Space Sci.* **51** 1–7
[61] Rosenberg M and Shukla P K 2000 Low-frequency Hall current instability in a dusty plasma *J. Geophys. Res.* **105** 135–9
[62] Izvekova Y, Popel S and Chen B B 2015 Nonlinear acoustic-gravity waves and dust particle redistribution in earth's atmosphere *J. Atmos. Sol.-Terr. Phys.* **134** 41–6
[63] D'Angelo N 2003 Hall instabilities in dusty plasmas *Planet. Space Sci.* **51** 393–8
[64] Havnes O, Aanesen T K and Melandsø F 1990 On dust charges and plasma potentials in a dusty plasma with dust size distribution *J. Geophys. Res* **95** 6581–5

[65] Brattli A, Havnes O and Melandsø F 1997 The effect of a dust-size distribution on dust acoustic waves *J. Plasma phys.* **58** 691–704
[66] Meuris P 1997 The influence of a dust size distribution on the dust-acoustic mode *Planet. Space Sci.* **45** 1171–4
[67] Duan W S and Shi Y R 2003 The effect of dust size distribution for two ion temperature dusty plasmas *Chaos Solit. Fractals* **18** 321–8
[68] Banerjee G, Maitra S and Dasgupta C 2015 New cutoff and resonance for dust acoustic waves in dusty mesosphere *Phys. Plasmas* **28** 012101
[69] Burns J A, Showalter M R and Morfill G E 1984 The ethereal rings of Jupiter and Saturn *IAU Colloq. 75: Planetary Rings* (Tucson, AZ: University of Arizona Press) 200–72 https://ui.adsabs.harvard.edu/abs/1984prin.conf..200B/abstract
[70] Fejer B G, Providakes J and Farley D T 1984 Theory of plasma waves in the auroral E region *J. Geophys. Res.* **89** 7487–94
[71] Pandey B P and Wardle M 2008 Hall magnetohydrodynamics of partially ionized plasmas *Mon. Not. R. Astron. Soc.* **385** 2269–78
[72] Pandey B P and Vranjes J 2006 Physics of the dusty Hall plasmas *Phys. Plasmas* **13** 122106
[73] Srivastava S, Mishra R and Sodha M S 2016 Modification of ionospheric electron density by dust suspension *J. Phys. D: Appl. Phys.* **49** 205503
[74] Rosenberg M and Shukla P K 2002 Dust-acoustic-drift wave instability in a space dusty plasma *J. Geophys. Res.* **107** SIA 21–1
[75] Rosenberg M and Shukla P K 2002 Parallel propagation effects on low-frequency Hall current instability in a dusty plasma *Planet. Space Sci.* **50** 261–7
[76] Gurevich A V 1978 *Nonlinear Plasma Phenomena in the Ionosphere* (New York-Heidelberg-Berlin: Springer-Verlag)
[77] Dimant Y S and Sudan R N 1995 Kinetic theory of the Farley-Buneman instability in the E region of the ionosphere *J. Geophys. Res.* **100** 14605–23
[78] Pandey B P and Vladimirov S V 2018 Dust modification of the plasma conductivity in the Earth's mesosphere *J. Atmos. Solar Terr. Phys.* **175** 24–30
[79] Vasyliunas V M 1970 Mathematical models of magnetospheric convection and its coupling to the ionosphere *Particles and Fields in the Magnetosphere* ed M Mc Cormac and D Reidel (Dordrecht, Netherlands: Springer) 60–71 https://link.springer.com/chapter/10.1007/978-94-010-3284-1_6
[80] Blanc M and Richmond A D 1980 The ionospheric disturbance dynamo *J. Geophys. Res* **85** 1669–86
[81] Igarshi K and Schlegel K 1987 Electron temperature enhancements in the polar E-region measured with EISCAT *J. Atmos. Terr. Phys.* **49** 273–80